

**Implementing Dynamic Foot Shape Models to Improve
Spacesuit Boot Fit**

by

Abhishektha Boppana

B.S., Case Western Reserve University, 2017

M.S., University of Colorado Boulder, 2019

A thesis proposal submitted to the
student's graduate committee in partial fulfillment
of the requirements for the degree of
Doctor of Philosophy

Ann and H.J. Smead Department of Aerospace Engineering Sciences

2022

Committee Members:

Dr. Allison P. Anderson, Chair

Dr. Torin Clark

Dr. David Klaus

Dr. Rodger Kram

Dr. Daniel Feeney

Contents

Chapter

1	Motivation	2
1.1	EMU Spacesuit Injury Incidence	3
1.1.1	Spacesuit Contact Injuries	4
1.1.2	Spacesuit Musculoskeletal Injuries	5
1.2	Hypothesized Spacesuit Injury Mechanisms	5
1.3	Spacesuit Injury Countermeasures	7
1.4	Summary	8
2	Background	9
2.1	Planetary Ambulation	9
2.2	Gas Pressurized Spacesuit Characteristics	11
2.2.1	An Inherently Stiff Structure	11
2.2.2	Mobility Design Features	12
2.3	MK III Ambulation Performance	13
2.3.1	Cost of Transport Factors	14
2.3.2	Ambulation Biomechanics	15
2.3.3	Subjective Feedback	15
2.4	Spacesuit Fit	16
2.4.1	Spacesuit Sizing Process	17

2.4.2	Quantifying Fit	18
2.4.3	Body Shape Characterization to Improve Fit	19
2.5	Summary	20
3	Investigative Approach	22
3.1	Expected Outcomes	26
4	Specific Aim 1 : Challenges in Quantifying Heel-Lift during Spacesuit Gait	28
4.1	Introduction	28
4.2	Methods	30
4.2.1	Data Collection	30
4.2.2	Data Analysis	31
4.3	Results	36
4.4	Summary	37
5	Specific Aim 2: Predictively model dynamic changes in foot morphology during gait	43
5.1	Introduction	43
5.2	DynaMo: Dynamic Body Shape Capture with Intel RealSense Cameras	45
5.3	Development of a Predictive Dynamic Foot Shape Model from Statistical Shape Modeling	47
5.3.1	Methods	47
5.3.2	Results	52
5.3.3	Foot Shape Changes	56
5.3.4	Study Limitations	60
5.3.5	Study Conclusions	61
5.4	Analysis of Dynamic Instep and Arch Height Changes	61
5.4.1	Methods	64
5.4.2	Results	66

5.4.3	Translating Instep and Arch Height to Footwear Design	68
5.5	Summary	71
6	Specific Aim 3: Define a design process integrating dynamic foot morphology data for a novel spacesuit boot	73
6.1	Introduction	73
6.2	Existing Knowledge on Foot Shape Mobility	74
6.2.1	Linear Anthropometry	74
6.2.2	Gait Joint Kinematics	75
6.3	Biomechanical Boot Design Framework	77
6.3.1	Mobility	78
6.3.2	Toe box	79
6.3.3	Upper	80
6.3.4	Sole	81
6.4	Prototype Planetary Spacesuit Boot Design	82
6.4.1	Ankle Convolute	84
6.4.2	Upper and Toe Box	88
6.4.3	Instep Lacing	90
6.4.4	Heel Counter	93
6.4.5	Sole	94
6.5	Novel Planetary Spacesuit Boot Construction	95
6.5.1	Ankle Convolute Construction	98
6.5.2	Upper and Toe-Box Construction	99
6.5.3	Sole Construction	100
6.5.4	BOA Lacing Integration	102
6.5.5	Heel Counter	102
6.5.6	Pressure Sealing	102

6.6	Classic Spacesuit Boot Design and Construction	102
6.7	Summary	103
7	Specific Aim 4: Evaluate novel planetary spacesuit boot design for fit, comfort, and mobility	106
7.1	Introduction	106
7.2	Test Interface Construction	107
7.3	Experimental Design	108
7.4	Stretch Testing Goals	109
7.5	Summary	110
8	Summary and Execution Plan	111
8.1	Publications	111
8.2	Academic Requirements	116
8.3	Timeline	116
Bibliography		118

Chapter 1

Motivation

The Apollo missions represent the last time humans set foot on another planetary surface, the Moon. Future human spaceflight missions are retargeting planetary surface exploration by sending astronauts back to the Moon and onward to Mars. While robotic missions can perform many of the scientific aspects of planetary exploration, human exploration still plays a key role in planetary mission success [42].

Spacesuits are designed to both provide life support and help protect the astronaut during activities conducted outside a space habitat, known as extravehicular activity (EVA). EVA is an important consideration of planetary exploration, allowing astronauts to perform scientific experiments, collect geological samples, perform habitat maintenance, and construct infrastructure. During EVA, astronauts are subject to many physiological and environment factors, including reduced gravity loading, dust, radiation, and extreme environment temperatures. In addition, the lack of atmosphere does not provide life support. Therefore, an EVA spacesuit's primary design objectives are to protect its operator from the environment and allow them to perform EVA tasks.

Humankind's current planetary EVA experience is limited to a total of 78 hours over 6 Apollo surface missions [114]. During the Apollo missions, astronauts performed almost 10 hours of EVA in a 24 hour period without the assistance of a rover during Apollo 14, and 22 hours of EVA in a 36-hour period with the assistance of a rover during Apollo 17 [114]. The longest traverse performed on the lunar surface occurred during Apollo 12, where astronauts Charles Conrad and Alan Bean walked 1.8 km [114]. Apollo 15-17 missions involving a rover assumed astronauts would be able to walk 5 km

in case of rover failure [114], but this requirement is doubled for future missions. Future planetary mission design assumes astronauts can walk up to 10 kilometers to return to their habitat, and that astronauts can perform 8-hour EVAs, with a limit of 12 hours of EVA per 24 hours and 24 hours of EVA per 7 days [42]. In addition, NASA's current planetary exploration plans focus on extended stays and colonization, increasing surface mission time and therefore increasing total EVA time. Future planetary EVA missions will therefore need a spacesuit that comfortably protects astronauts while they perform EVA tasks and traverse across the surface on these long duration missions.

1.1 EMU Spacesuit Injury Incidence

Following the Apollo era, space missions have all occurred in low Earth orbit in a microgravity environment. New spacesuits, such as the Extra-Vehicular Mobility Unit (EMU) were designed for microgravity operations. This included greater upper-torso mobility while reducing lower-torso mobility, as astronauts would be floating in space and not be required to ambulate. However, the increase in EVA activities that accompanied the construction of the International Space Station have increased the incidence rates and severity of crew injuries, prompting studies into the human-spacesuit interactions and deficiencies in suit design that lead to these injuries.

Crewmember difficulties with the spacesuit have existed since the first EVA, where Alexi Leonov had difficulties moving the suit to re-enter the spacecraft. Apollo astronauts have commented on the fatiguing reduced mobility of their spacesuits [125]. Gas pressurized spacesuits are known to be inherently stiff and rigid [111, 1, 128, 68], difficult to move [105, 5], and have the potential to cause injuries both during operations and ground-based training [152, 137, 125, 126, 10, 32].

The prevalence of injury has been well studied in the era of on-orbit microgravity EVAs performed with the EMU. Strauss [137] found that 24.6% of training sessions at the Neutral Buoyancy Laboratory (NBL) between 2004 to 2006 study had reported injury symptoms. Viegas [145] found a 67.5% reporting rate of injury symptoms from astronauts training in the NBL between 2002 to 2003. An in-flight injury incidence of 0.24 was reported by Scheuring [127] for EVAs occurring on

Space Shuttle flights 90 to 113. These injuries can be classified as contact injuries, including bruises and abrasions; and musculoskeletal injuries, including muscle tears, strains, and inflammation.

1.1.1 Spacesuit Contact Injuries

Spacesuit contact injuries have been the most reported operational injury mechanism in the US space program [125], and in the EMU [137, 145, 127]. Contact injuries occur through repeated contact between the wearer and the spacesuit. High contact pressure between the wearer and spacesuit can lead to bruises, while shear can lead to abrasions [89, 26].

EVA hand injuries have been reported since the Apollo era, with symptoms including swollen and abraded joints, putting the mission at risk [127]. Hand injuries continue to be most frequently reported injury in the EMU [137, 145, 127]. Hand contact injuries include fingernail delamination, abrasions, contusions, and nerve impingement [137, 145, 127]. These injuries have widely been attributed to the poor fit and unprotected contacts between the hand and the spacesuit glove [137, 145].

Shoulder contact injuries occur from the combination of unprotected contact and high weight loading in the EMU [137, 145, 10]. Shoulder injuries are reported as the second most common EMU injury location and frequently occur during ground-based training in the NBL, when the wearer may be inverted in the suit [137, 145]. While the suit and operator together are made neutrally buoyant, the operator is able to shift relative to the suit due to gravity. Therefore, they “fall” into the suit, and are now making contact with the hard upper torso (HUT). Therefore, the increased contact and high levels of load leads to shoulder contact injuries.

The feet are the next most reported areas of in-flight EMU contact injuries in the spacesuit [127]. Traditionally, not much motion occurs in the lower torso of the EMU spacesuit due to its design targeting microgravity operations. The feet are normally restrained in a fixed foot restraint, while the astronaut performs tasks utilizing their upper body. One astronaut reported a “searing, knife-like pain” on their foot during on-orbit EVA which was unable to be rectified [127]. This resulted in a blister and decreased sensation on the foot’s dorsal surface, and was later attributed

to having excess pressure bladder material in the boot [127]. Strauss [137] also reports contact injuries on the toes and dorsal surface stemming from the boot sizing insert, which does not adequately project the astronaut from contact from the foot restraint or bladder folds.

Other reported locations for EMU contact injuries include the elbow, knee, and trunk [137, 127]. Injuries at wearer's elbows and knees are reported to come from rubbing against the convolute joints [137]. Injuries at the trunk are reported to occur from contact between the wearer's back and the Liquid Cooling and Ventilation Garment (LCVG) in the spacesuit [137].

1.1.2 Spacesuit Musculoskeletal Injuries

Fatigue from high exertion may lead to musculoskeletal injuries EMU Musculoskeletal injuries have been reported in the hands, due to the high exertion needed to actuate fingers on the pressurized glove [145]. Fatigue may occur after many hours of completing EVA tasks [137, 127]. Similarly, the elbow joints in the EMU have also reportedly caused strains [137].

Limitations of the EMU suit design can also lead to musculoskeletal injuries, the most severe which occurred at the shoulder [137]. EMU operators can overuse their rotator cuff during EVA tasks, leading to muscle strains, sprains, tears, and overuse injuries [152, 137, 138, 127]. Some of these injuries have required surgical intervention [138].

1.2 Hypothesized Spacesuit Injury Mechanisms

Limitations in suit joint design and the poor fit between the suit and its operator can both lead to contact or musculoskeletal injuries. While other environmental factors, such as increased humidity, were also found to have a role in EMU fingernail de-lamination [32], this section will focus on the design and fit factors for spacesuits. High exertion needed to actuate joints and poor indexing can lead to excessive musculoskeletal injuries, while poor sizing and poor indexing can lead to contact injuries, increasing the risk of injury fig. 1.1.

Pressurized spacesuit joints require more energy to move than compared to unsuited motions [102, 5]. While design features aim to reduce the effort needed to bend joints [65], these joints are

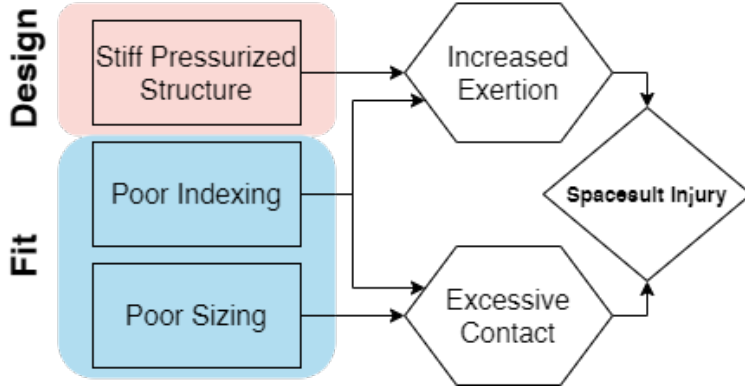


Figure 1.1: Overview of how deficiencies in spacesuit design and fit can lead to increased injury risk

difficult to engineer in areas such as the hand. Therefore, the fatigue and strain injuries reported in the hand could be due to inherent design deficiencies of EMU spacesuit gloves [137, 145].

Spacesuit joints also need to be properly aligned to the wearer to reduce both contact and musculoskeletal injury risk. Indexing is a specific fit measurement regarding the alignment of the operator's joints to the spacesuit's joints. Poor indexing can lead to contact injuries when suit-operator joint centers become misaligned and cause rubbing against the suit during motion, as seen in the elbow and knee of the EMU [137]. Deficiencies in suit design, including the high exertion to actuate joints and range-of-motion limitations, can also cause poor indexing and lead to injury. Viegas reports a specific mechanism in the EMU glove where the high exertion required to actuate the glove results in dorsal displacement of the metacarpophalangeal joints, pushing the tops of fingers against the surface of the glove and causing inflammation [145]. Poor indexing at the the EMU HUT design forces internal rotation of the shoulder due to the scye opening not allowing for full range-of-motion of the shoulders, leading to potential overuse and injury of the rotator cuff muscle [152, 137, 138, 127]. Suit joints should therefore be designed and sized to ensure proper indexing.

Suit components also need to be properly sized to the operator to reduce contact injury risk. Sizing, along with indexing, ensures that the suit is fit to the operator. Spacesuits in the Apollo era were custom tailored to each astronaut. However, as the astronaut corp grew, the EMU presented a modular sizing system, where differently-sized suit components had to be selected for

each astronaut. Gaps between the wearer and the spacesuit could lead to excessive contact when the wearer moves and shifts inside the spacesuit [16]. Suit components which are too small can also cause higher contact pressures, leading to potential contact injuries [9]. Poorly sized bladder inserts were found to be a factor in EMU foot injuries [137]. Opperman et al. [108] found that higher hand circumferences have a larger incidence of fingernail delamination in the spacesuit glove, while Charvat et al. [33] found smaller hand circumferences to be a risk factor in fingernail delamination, showing how sensitive fit is in leading to injury. Suit components should therefore be sized accurately to the suit's operator to ensure proper fit.

1.3 Spacesuit Injury Countermeasures

Attempts to mitigate spacesuit injury have focused on addressing the fit and mobility limitations of the EMU. Newer spacesuit prototypes feature larger scye openings for better indexing and more mobile shoulder bearings compared to the EMU [61]. However, testing of microgravity EVA task performance in the NBL found that while the new design allowed for more shoulder compatibility, larger subjects still reported discomfort in the shoulder area [94]. This shows how sizing and indexing are just as important as spacesuit mobility to ensure a properly compatible spacesuit. It still remains impossible to perfectly fit every person to the EMU spacesuit due to the wide ranges of anthropometry and limited sizing components [16]. Back padding on the EMU was found to potentially assist wearers in controlling the upper torso of the suit, reduce over-rotation of the torso to keep upper extremity joints aligned, and improve indexing at the gloves [32]. For wearers with a smaller anthropometry however, indexing at the hip bearings was unable to be fixed by padding, due to the limitations in torso length. In addition, effects of indexing on performance are inconclusive [48]. Therefore, there is a need to improve spacesuit sizing and indexing to work with any improvements in spacesuit mobility to reduce the risk of contact and musculoskeletal injuries.

1.4 Summary

The push towards planetary exploration requires advancements in spacesuit design to create a safe and comfortable environment for astronauts to perform EVAs. Our planetary exploration experience is limited to just 6 Apollo missions to the Moon as missions have shifted towards microgravity research, but future plans call for an extended human presence on the Moon and Mars. Microgravity EVAs and training have resulted in many upper torso injuries due to hard-to-move joints and poorly fitted suits. The transition to planetary EVAs, with a focus on ambulation, may result in a higher incidence rate of injuries in the lower torso without significant changes in the way spacesuits are designed and fitted. Therefore, it is important to understand how operator-spacesuit interactions and spacesuit performance may lead to injury in the context of planetary tasks such as ambulating as planetary surface missions are planned. This will allow for the construction of safer and more comfortable spacesuits to reduce the risk of injuries during EVA.

Chapter 2

Background

Poor suit design and suit fit are two of the main suit variables leading to injury risk and compromised performance during EVA [32]. Pressurized spacesuits will continue to be used for EVAs through the transition from microgravity to planetary exploration, and therefore will require improvements to their joint design and fit to ensure safe and comfortable EVA. As future missions target planetary exploration, ambulating across the surface becomes a critical EVA task, and requires an understanding of reduced-gravity ambulation and suited effects on ambulation. There are also many challenges that are associated with fitting spacesuits which have not yet been solved. This chapter introduces how current suits perform in planetary ambulation and introduces the challenges with fitting spacesuits.

2.1 Planetary Ambulation

Walking is not always the most energetically preferable gait. Astronauts during the Apollo missions did not walk while traversing the surface; they famously loped across the surface. In fact, loping is the energetically preferred gait on the Lunar surface, while walking, skipping, and running are energetically preferable on Mars [2]. As speeds increase in lunar gravity, a transition occurs from walking to skipping rather than from walking to running as on Earth [96]. However, the energetically preferred speed is not always achievable or possible, and slower walking speeds may be necessary when performing EVA tasks.

Studying the walk-run or walk-skip transition gives further insight into ambulation on a planetary surface. Walking is modeled as an inverted pendulum which conserves some energy between each step; but energy is not conserved at faster walking speeds and needs muscular power input [30, 29]. Griffin et al. [62] found as gravity is reduced, the amount of mechanical energy conserved between each step is reduced, and the maximum energy recovery occurs at slower speeds. Ivanenko et al. [70] found that muscle activation and ground contact forces decreased with lower gravity levels, but kinematic coordination of the lower limbs were not affected by gravity levels. The Froude number is the ratio between the centripetal and gravitational forces in the inverted pendulum model, as shown in eq. 2.1.

$$Fr = \frac{v^2}{gL} \quad (2.1)$$

Where Fr is the Froude number, v is the velocity of ambulation, g is the gravitational force, and L is the leg-length [3]. At some critical value, walking is theoretically impossible as the gravitational force cannot match the required centripetal force, which is where the walk-run transition occurs (Fr^*). Humans typically switch to running at $Fr = 0.5$. Kram et al. [82] offloaded subjects by their waist as they walked and ran on a treadmill, and found that Fr^* increases at lower gravity levels. The increase in Fr^* was hypothesized to be from the arms and legs not being offloaded and still under the influence of gravity [82]. Donelan and Kram [41] also found that elastic forces were unable to predict the dynamics of reduced-gravity running. This suggests that other factors may be at play with walking in reduced gravity.

Ambulating with the suit involves additional forces both applied by the suit, and applied by the user to control the suit. Newman and Alexander [103] suggested that energy may be expended at low speeds and lower gravity levels for stability and postural control for ambulation. Chappell [31] found that when the offload system was set to lock waist rotation for stability, subject's gait was constrained and showed changes in braking and propulsion force for Lunar gravity. Therefore, stability is an important factor in walking at lower gravity levels.

Carr and McGee [27] developed the Apollo number Ap to explain the effects of the space-suit's pressure forces on gait (eq. 2.2).

$$Ap = \frac{Fr}{M}, \text{ where } M \text{ is the mass ratio of the spacesuit.} \quad (2.2)$$

M incorporates the self-supported weight of the spacesuit. The self-supported weight of the spacesuit is from the spacesuit's pressurization. Carr and McGee validated the Apollo number against gait events during Apollo missions, but found that the Apollo number did not fully explain the walk-skip transitions. **Therefore, a gas-pressurized spacesuit's mobility restrictions and joint mechanical work, along with its pressure forces, may also be affecting suited ambulation.**

2.2 Gas Pressurized Spacesuit Characteristics

2.2.1 An Inherently Stiff Structure

Gas pressurized spacesuits have been used for all EVAs throughout the history of human spaceflight. However, gas pressurized suits become stiff and rigid when pressurized, requiring great effort to bend. The first EVA spacesuit, the Gemini suit, did not include any design features to reduce bending effort [139]. If a gas pressurized suit component is represented as a pressurized cylinder, bending the cylinder along its axis causes a reduction in volume at the bend [65]. As a result, pressure at the bend will increase, causing resistance to the bending force. The force required to change the volume at the bend is presented in eq. 2.3 [102, 65],

$$F = \frac{W}{d} = \frac{\frac{p\pi D^3 \phi}{8}}{\frac{L\phi}{2}} = \frac{p\pi D^3}{4L} \quad (2.3)$$

where F is the force required, W is the work required, d is the distance the joint is flexed, p is the pressure, D is the cylinder's diameter, ϕ is the joint deformation angle, and L is the length of the cylinder. It can be seen that the force required to bend a pressurized joint is not dependent on the bending angle, but rather the length and diameter of the pressurized section. Without dedicated

mobility features to maintain a constant volume at joints, the forces required to bend representative spacesuit components can be as high as 200 lbs for the waist joint [102].

2.2.2 Mobility Design Features

Mobility design features allow for bending of a pressurized joint by creating a point at which the joint can buckle, and allowing the joint to maintain constant volume through the bending motion [65]. This greatly reduces bending resistance and allows for joint flexibility [65]. These mobility features typically feature some form of bellows or convolutes to maintain constant volume and axial restraints to prevent elongation of the joint under pressurization [65].

Mobility design features have been studied and iterated since the advent of space travel, but were not implemented in the Apollo mission suits. The Litton company built and tested spacesuits for EVA use in the 1950s, predating both the US and Russian space programs. These suits iterated on the use of convolutes by inventing the rolling convolute, annular convolute, and cardonic hard joint [65]. While these suits never saw operations on spaceflight, they did prove benefits in mobility over the International Latex Corporation (ILC) designed A7L suits, which were eventually used by US astronauts on the moon. The Litton suits were able to match the center of restraint and center of pressure when convolute joints were bent, reducing the bending torque and spring return force of the joint [65]. Therefore, the suit's operator is able to easily bend the joint and not exert much force to keep the joint bent. The A7L suit's convolute joints did not match the center of restraint and center of pressure, requiring operators to exert additional force to both bend the joint and keep it bent [65]. Such drawbacks of the A7L suit required astronauts to come up with clever workarounds. On an Apollo 16 EVA, astronaut John Young found that “by hopping into the air and landing on his feet, the weight of his suit overcame the suit’s internal pressure, so he could get to his knees and pick up rocks without using geological tools” [114]. Integrating convolutes into the A7L suits may have improved mobility on the Moon.

Advancements since the Apollo era have brought us improvements in pressurized joint design to increase mobility, including the toroidal mobility joint, dual-axis joint, hard component joints,

hybrid hard-component/fabric joints, and improvements to flat-patterned joints [65]. The Mark III Advanced Space Suit Technology Demonstrator EVA Suit (MK III) is a spacesuit designed by NASA as a planetary spacesuit design testbed [80]. These advancements have allowed for increased lower-torso mobility as shown in the MK III spacesuit technology demonstrator; operators are easily able to recover from a fall and kneel in the MK III while these tasks were done with much difficulty in the A7L and EMU spacesuits [79].

Lessons from EMU and MK III design were applied to the design of the new Z2 planetary spacesuit prototype. The Z2 prototype was first developed by NASA and ILC Dover in 2016 to demonstrate planetary surface exploration technologies, but parts of the Z2 suit are now being used for the Exploration EMU (xEMU), to supplement or replace the EMU for ISS EVAs [61, 94]. The Z2 also serves as the basis for the design of the Artemis spacesuits, which will be worn by the first crew to step foot on the Moon. The Z2 spacesuit features a larger scye opening and more mobile shoulder bearings compared to the EMU [61]. Tests of the Z2 in the NBL found range-of-motion and reach envelope improvements over the EMU, but many microgravity EVA tasks were reported to be harder and more limited in the Z2 [94]. Subjects also reported similar muscle fatigue and exertion ratings between the EMU and Z2 [94]. Larger subjects also reported discomfort in the shoulder area, further highlighting the importance of fit in spacesuit design [94]. Similar analysis needs to occur with ambulation to assess the effect of suit mobility improvements.

2.3 MK III Ambulation Performance

The MK III spacesuit has been used to experimentally study suited effects on ambulation due to the Z2's relative novelty. In the EVA Walkback Test (EWT), six male subjects were tested with the MK III spacesuit on a treadmill to explore the effects of the MK III spacesuit's weight on planetary ambulation in Lunar (1/6g) and Martian (3/8g) gravity levels. Subjects were tested in three conditions: unsuited and offloaded to selected gravity level; unsuited and offloaded to selected gravity level with the suit weight matched; and suited while offloaded to selected gravity level [105]. This allowed for analysis of suit weight separately from other suit design factors on the

metabolic cost of suited ambulation. Subjects were tested at three speeds above and three speeds below their walk-run transition speed. All subjects also did a 1G baseline unsuited trial and a 10 km suited lunar ambulation. A follow-on integrated suit test (IST) examined the effects of varied suit mass, gravity, and on metabolic cost and kinematics on Lunar suited gait [104] with similar conditions while varying suit pressure and mass. These and similar tests provide insight into how the MK III's design factors affect suited ambulatory performance.

2.3.1 Cost of Transport Factors

Metabolic cost of transport, a measure of how much energy the body is exerting during ambulation calculated through direct calorimetry [74], was collected in these tests across a variety of conditions. Metabolic cost is a direct measure of how hard the body is working to move in the spacesuit. Previous studies have shown that the metabolic cost of transport decreases with gravity [58]. Findings from the EWT and IST were consistent with these previous findings [105, 104]. Unsuited weight-matched metabolic costs were lower than 1G unsuited across all speeds for 1/8G ambulation and similar to 1G unsuited for 3/8G ambulation [105]. This suggests that without suit effects, ambulation on Mars may be metabolically similar to ambulating on Earth. However, the MK III increased the metabolic cost of transport for both gravity environments compared to the unsuited weight-matched condition [105]. At 1/6G, the MK III had a higher metabolic cost than Earth ambulation at lower speeds, but was less metabolically costly at higher speeds [105, 104]. The MK III was very metabolically costly in 3/8G, metabolic cost quickly approach maximal values for low speeds and subjects were unable to run in the suit at higher speeds [105]. The metabolic cost of weight (5%-13%) for both Lunar and Martian gravity levels was significantly dwarfed by the cost of suit design factors (87%-95%) [105]. From these results, its apparent that the MK III's design cannot service ambulation on Mars due to its design factors, but may be sufficient for the Moon.

Other suit design factors partially explained the increased metabolic cost of suited ambulation. The IST found increased suit pressure to minimally increase metabolic cost across all speeds, hypothesized to be due to the MK III's constant volume joints [104]. However, there were some sub-

jective differences in mobility noted across the different pressures, although there was no correlation to subject anthropometry [104]. The effect of suit weight, which encompasses gravity level and suit mass, steadily increased with speed [104]. The percentage of metabolic cost that was not explained by suit weight or pressure decreased as speed increased, but then increased at the fastest speed [104]. Additional factors which can explain the increased metabolic cost can include suit kinematics, stability, and harnessing effects from the gravity offloading, which may be causing more difficulty for ambulation at lower speeds. However, these factors were not isolated in the MK III ambulation experiments. The majority of ambulation during an EVA is most likely done at lower speeds, thereby requiring further understanding of how suit design is affecting mobility at low speeds.

2.3.2 Ambulation Biomechanics

The IST captured little differences in kinematics as a function of pressure, which may be due to the constant volume joints [104]. However, it was noted that at 4.3 psi, the knee joint was limited by the design of the pressurized suit, and that the ankle increased its range-of-motion (ROM) to compensate the limited knee ROM [104]. This shows the importance of the kinematic chain in suited mobility; when a certain motion is inhibited, other joints along the kinematic chain will have to compensate. Similar compensation has led rotator cuff injury in the EMU's HUT [152].

Cullinane et al. [37] found suited MK III ambulation at 1G to reduce heel and toe clearance above ground compared to unsuited ambulation. In addition, the MK III was found to decrease speed, stride length, and step length compared to unsuited ambulation [37]. Cadence and stance time increased with gravity level in the IST, consistent with how metabolic cost increases with gravity level [104]. These findings suggest that the MK III inhibits operator mobility and agility when ambulating.

2.3.3 Subjective Feedback

Subjective feedback allows operators of the MK III to provide their perception of ambulating in the suit. Rating of Perceived Exertion (RPE) and Gravity Compensation and Performance Scale

(GCPS) were consistent with metabolic cost findings in both the IST and EWT; both increased with gravity and speed [105, 104]. Subjects performing the 10 km suited lunar ambulation in the EWT reported “fair” to “moderate” operator compensation required to walk in the MK III on the Cooper-Harper Scale [105]. While mean rating of discomfort was “very low” to “low” on the Corlett-Bishop Scale, discomfort and trauma were noted on the knees and feet of some subjects [105] (fig. 2.1). In addition, muscular fatigue and tightness was also reported in the quadriceps, thighs, glutes, and lower back [105].

Subjective feedback for ambulating in the MK III at 1/6-g suggests that it is mostly acceptable for lunar ambulation. However, the reported trauma and musculoskeletal discomfort are areas of concern. The EWT and IST, along with findings from Cullinane et al. [37], show that the MK III’s design inhibits natural human motion and requires more effort during suited ambulation. It is not enough, however, to design a suit that more closely matches natural human motion; it also needs to work closely with its operator to reduce injury risk from poor fit.



Figure 2.1: Knee (left) and foot (right) trauma identified in the MK III following 10 km walkback evaluation. From Norcross et al. 2009

2.4 Spacesuit Fit

Spacesuit mobility needs to have matched spacesuit-operator interaction, primarily driven by spacesuit fit, to ensure the suit works with its operator. Proper spacesuit fit requires both correct sizing and correct indexing between the spacesuit and its operator. In addition, these factors must be maintained not only in a static pose, but through dynamic movements as well.

Static fit refers to the alignment between the operator and the spacesuit, while dynamic fit refers to the coordination of the operator to the spacesuit during motions [135]. Poor static fit leads to empty space around the operator, which allows the operator to move inside and repeatedly contact the spacesuit. However, improving static fit is not as easy as filling this empty space; this would hamper operator mobility and lead to poor dynamic fit and difficulty for the operator to move the suit. In addition, the effect of fit on suited performance is difficult to understand. Difficulty in both sizing the suit and ensuring that suit movements match operator movements may be further improved through body shape modeling.

2.4.1 Spacesuit Sizing Process

The Apollo EVA spacesuits were custom tailored for each individual, a feat achievable with the small number of astronauts needing EVA suits [65]. However, with a larger and more diverse astronaut corp, custom suits became infeasible. Currently, only the EMU glove is custom made if one which fits the astronaut does not exist [32]. NASA STD-3000 calls for spaceflight hardware to accommodate an anthropometric range from the 5th-percentile female to the 95th-percentile male [100]. The EMU suit was designed to target this range with modular and adjustable components. However, the EMU design only ended up fitting a 40th-percentile female to a 95th-percentile male [77]. In addition, it is not clear what measurement is used to define the population percentiles that the EMU fits.

Even with some adjustable sizing components in the EMU, it takes experienced suit engineers to select and adjust the size of EMU components to best fit the operator. Sizing rings are used in the EMU design to change the length of components like arms and legs [65]. Sizing inserts such as pads can also help position the operator within the spacesuit [32]. The length of restraint straps at convolute joints can be adjusted to change the length of soft components, but this affects joint mobility as the length-diameter ratio is modified [65]. Current suit fit processes do not use any objective measures to define proper fit; a baseline fit is prescribed from anthropometric measures

and then iterated through subjective feedback [47]. Fit is inherently difficult to objectively measure due to the challenges of measuring operator motion inside the suit.

2.4.2 Quantifying Fit

Novel measurement technologies have been explored to measure operator motion inside the spacesuit as traditional optical motion-capture techniques cannot be used through the spacesuit. Pressure sensors can help quantify contact between the operator and spacesuit and highlight hotspots of contact which can indicate poor fit [7, 8, 9]. Inertial-measurement unit (IMU) systems aim to provide some insight into how the operator is moving relative to the suit [18, 48, 131]. Fabric strain sensors have also been developed to predict an operator's body-shape inside the spacesuit [77].

Fineman et al. [48] introduced two objective fit metrics which can help characterize poor static and dynamic fit in the spacesuit: difference in knee angle ROM between the suit and operator, and the relative coordination metric [49]. The relative coordination metric allows for the identification of whether the suit or the operator is driving the other component. Fineman et al. [48] measured these metrics with IMUs placed on the lower torsos of both the operator and the spacesuit. Three subjects walked in a spacesuit with different levels of padding, meant to mimic three different levels of fit. Two subjects had reduced knee ROM compared to unsuited ambulation. One subject had no significant differences in metrics between padding levels but reported better responsiveness with higher levels of padding. Another subject had the lowest knee ROM with no padding, aligning with their feedback that higher levels of padding are harder to control. Results from this study show how some performance metrics can measure the effects of varying fit, but also how fit is very subjective.

Suit fit engineers have commonly reported a dynamic fit problem where the heel lifts out of the boot during heel-off, as shown in Figure 2.2. This was also reported by one subject in Fineman et al. [48]. Data collected from Fineman's study shows that during heel-off, the suit appears to be driven by the operator at the calf. While this may suggest heel-lift, it does not corroborate the subjective reports of a gap between the operator's heel and the spacesuit's heel

as it cannot directly measure this gap. Fineman et al [48] suggests that boot fit may be very important to ambulating in the MK III spacesuit.



Figure 2.2: Heel-lift occurring during heel-off, as subjectively reported in the MK III. The poor fit and indexing in the boot and lower torso allows the heel to lift inside the boot during heel-off

2.4.3 Body Shape Characterization to Improve Fit

NASA's Anthropometry and Biomechanics Facility (ABF) has focused on characterizing the human body as it relates to spacesuit fit. Linear measurements are traditionally used in sizing algorithms to determine a baseline suit fit. These linear measurements are then compared to linear measurements in the suit's design to determine appropriate sizing components. However, linear measurements do not always accurately represent a person's body shape [91]. Three-dimensional scanning can help accurately characterize body-shape to allow for virtual fit testing against 3D models of the suit. Boundary manikins can be generated which represent the extremities of accommodated anthropometry, and overlaid on 3D suit models to determine fit [91]. Virtual fit check metrics may include penetration depth, contact areas, and overlap volume [77]. Monte-

Carlo simulations of vast databases can also be virtually tested to find fit problems that may occur outside the boundary manikins [77].

However, static body shape may not be enough to ensure dynamic fit. It is well known that parts of the body change shape during movement. Capturing 3D-scans in multiple poses also allows for the development of a parametric models that can estimate how body shape changes with a specific movement; for example this can be used to check for shoulder clearance around the HUT [78]. This can greatly improve dynamic fit as it ensures the HUT accommodates the shoulder throughout its entire motion. However, this methodology is limited to poses where the subject can pause between motions due to technological limitations for capturing dynamic body shape changes.

Body shape changes can also occur from exposure to an altered-gravity environment. The ABF found on average posture to increase by a maximum of 3%, hip circumference to decrease by a mean of 7%, and thigh circumference to decrease by a mean of 10% during microgravity spaceflight [77]. EMU sizing incorporates a 2.54cm increase in torso length to accommodate this change [140].

Information from virtual fit testing can be incorporated into spacesuit design by informing where the internal geometry may need to be expanded or contracted to better fit the target population [77]. This process was used to validate the design of the Z2 suit. However, it is virtually impossible to incorporate personal preferences of fit into this process; currently a threshold is implemented to determine acceptable levels of ease or compression [77]. In addition, modifying design to accommodate findings from fit can only be done to a certain extent; there are limitations on modifying the structure of an existing design while still meeting the same engineering requirements. There are also no clear metrics for translating virtual fit testing into spacesuit component design, and current methodologies are limited to modifying the design of existing components rather than designing new components from the ground-up.

2.5 Summary

Ambulating on another surface and gravitational environment presents many challenges of its own, including changes in preferred gait patterns. Wearing a stiff, pressurized spacesuit further

increases the effort required to walk. While constant volume joints may reduce pressurization effects, unquantified factors such as poor operator-spacesuit interaction may also be leading to injury. Spacesuit fit is hard to characterize due to limited knowledge of in-suit motion and challenges including limited suit sizing components, limited suit design flexibility, an incomplete understanding of body shape changes, and lack of quantifiable metrics to validate fit. Poor fit can reduce performance and lead to injury. Ambulation specific fit issues, such as heel-lift, have been subjectively identified in the MK III but not fully quantified. While there has not been a large scale study on injuries in the MK III, these fit issues are similar to the injury mechanisms leading to injury in the EMU.

Body-shape models have been proposed as a way to better fit operators to spacesuits. Static body shape models allows for correctly sized spacesuit components to be selected and spacesuit component designs to be validated for accommodation of a target population. Dynamic body shape models will ensure that dynamic fit is ensured throughout suit motions, but current technology is limited to capturing low-frequency motions. In addition, there is no established framework for integrating dynamic body-shape models into the spacesuit design process. Suit components designed around dynamic body shape models have not yet been tested for increased fit and comfort compared to traditionally designed and fitted suit components.

Chapter 3

Investigative Approach

The following gaps were identified from the previous research, as outlined in the literature review presented in the previous two chapters, and ~~will~~ motivate the direction of this thesis.

- **Gap 1:** Few efforts to quantify fit discrepancies

- * Subjective reports are currently used to identify fit discrepancies. While objective fit metrics can indicate decreased performance from poor fit, they cannot identify or confirm specific indexing discrepancies between the operator and spacesuit to support these specific reports.

- **Gap 2:** Limited knowledge on dynamic body shape changes due to motion

- * Current modeling of dynamic body shape relies on 3D capture of subjects pausing through the motion and interpolation of body shape between pauses. Technological challenges make it difficult to optically capture dynamic body shape changes where the subject cannot pause between the motion, such as during walking. Therefore, the lack of data makes it difficult to model these dynamic body shape changes.

- **Gap 3:** No existing framework for incorporating dynamic body-shape models into the spacesuit design and fit process

- * It is unclear how dynamic body shape models can be incorporated into both the design of spacesuit components, as well as used to virtually fit test proposed spacesuit

components. Current efforts have proposed ways to modify currently designed space-suit components, but not ways in which spacesuit components can be designed from scratch around dynamic body shape models.

- **Gap 4:** No studies to quantify the effect of using dynamic body-shape models over linear measurements on fit and mobility
 - * Spacesuit components designed around body shape models have not been tested against traditionally design spacesuit components to show that they result in better fit and mobility.

This proposed thesis will investigate the applicability of dynamic body shape models to improve fit and mobility for planetary EVA suit design. To limit the scope of the work, the proposed work will focus on fit and mobility of the spacesuit boot. The MK III spacesuit currently uses a pressurized modified hiking boot with a convoluted ankle joint and boot sizing inserts. The boot is an important component for MK III ambulation and MK III boot fit has been identified as a key issue in suit fit, especially with the subjectively reported instances of heel-lift [48]. While the thesis will focus on the foot-boot interface design, the novel contribution lies in the development of a experimental and design framework to translate body-shape changes into spacesuit design variables. The proposed hypothesis of this work is therefore:

Integrating dynamic body shape changes into the spacesuit boot design process will mitigate factors that lead to injury and improve compatibility between the operator and the spacesuit.

The proposed thesis will encompass the following specific aims:

- **Specific Aim 1:** Quantify instances of heel-lift in spacesuit gait
 - * **Motivation:** Heel-lift was subjectively reported as a potential symptom of poor fit during gait in the MK III, but was never quantified. Quantifying the ~~level frequency and magnitude~~ of heel-lift ~~may lead to heel-lift can better inform bootdesign to~~

~~mitigate this issue~~ can help understand the interactions between the human's foot and the spacesuit boot.

- * **Summary of Work:** ~~Walking data was collected on the MK III by Fineman et al. 2018. This data was reanalyzed in the context of boot fit by analyzing vertical Vertical accelerations of the spacesuit's lower leg and operator's tibia . Heel-off times were detected using vertical accelerations. An analysis was conducted on quantifying displacement from vertical accelerations, but was found to have large margins of error . Therefore, this work proposes differences in heel-off times as an indicator of were analyzed from IMY data collected on in the MK III suit by Fineman et al. [48]. Differences in heel-off times between the human and spacesuit were used to characterize heel-lift and identifies a methodology directly quantify instances. Drift correction techniques were implemented and evaluated to reduce error in integrating acceleration data to positional estimates. Results from both these analyses, however, suggest that IMUs may not be appropriate for quantifying heel-lift in future work magnitude and frequency.~~

- **Specific Aim 2:** Predictively model dynamic changes in foot morphology during gait

- * **Motivation:** The foot changes shape during the loading process of stance phase. Modeling these changes as they relate to subject anthropometry and kinematics will allow for prediction of dynamic foot shape during stance phase.
- * **Summary of Work:** A novel dynamic foot scanning system was developed to capture 4D foot scans from subjects walking on a treadmill. Dynamic foot scans were captured from thirty subjects as they walked on the treadmill. A predictive statistical shape model was developed to predict dynamic foot shape with an accuracy of 5.2 mm. From the model, the ~~midfoot arch~~ was found to ~~decrease in girth as the foot is lifted through heel-off. Dynamic changes in the midfoot will be further studied across the population as it relates to instep height and instep girth drop in height through stance~~

phase, and rise just prior to toe-off. An additional analysis to assess the relationship between arch height measures and subject anthropometries found little correlation, and therefore suggested that dynamic arch height measurements are highly subject specific.

- **Specific Aim 3:** Define and validate a design process integrating dynamic foot morphology data for a novel spacesuit boot

* **Motivation:** Existing knowledge on foot mobility can provide mobility requirements for a planetary spacesuit boot. Insight from the dynamic foot shape model can be integrated with these mobility requirements to develop a boot design that accommodates the mobility and dynamic shape of the boot.

* **Summary of Work:** Mobility of the foot was characterized from the existing literature. A biomechanical design framework was developed to integrate these mobility requirements with the dynamic foot shape model developed in Specific Aim 2. This framework ~~will be used to create a pressurized planetary spacesuit boot prototype. was then used to inform the design of a novel spacesuit boot by implementing a novel lacing feature which accommodates variability in arch height. The pressure bladder for a novel spacesuit boot accommodating this design feature was constructed, and tested to achieve a pressurization of 3.0 psi.~~

- **Specific Aim 4:** Evaluate the prototype planetary spacesuit boot design for fit, comfort, and mobility

* **Motivation:** The planetary spacesuit boot design developed in Specific Aim 3 will be tested for improved fit and comfort as compared to a current MK III spacesuit boot design and a non-pressurized standard ~~hiking work~~ boot. This will directly test the hypothesis of this thesis.

* **Summary of Work:** ~~The test subject will perform ROM tests in a glovebox with a vacuum, which will pressurize the boot. The subject will also perform heel lifts against~~

a false floor simulate the heel-off phase of gait. Kinematics of the ankle and MTP joint will be captured. Methods from SA1 along with a contact sensor in the heel of the footwear will check for the A pressurization interface around the subject's calf was constructed for both spacesuit boots to be tested. The test subjects performed heel-lift . Subjective surveys will assess the subject's fit and comfort levels. If the prototype boot design can achieve pressurization around the foot outside the glovebox, gait kinetics and kinematics will be captured with all three designs. The prototype boot may also be tested in conjunction with a full spacesuit , pending spacesuit testing availability. and walking motions in the all tested boots. A force sensor was integrated into the boots to measure heel contact through the motions. Subject discomfort and exertion was evaluated for each of the boots through surveys.

Analysis of heel-off times to indicate heel-lift has been completed in Specific Aim 1. A dynamic foot scanning system was developed, and used to create a predictive dynamic foot shape model in Specific Aim 2. This model is being used to study midfoot dynamic changes as they relate to population instep height and instep girth measurements. The design framework has been defined in Specific Aim 3, and prototype boots are currently being iterated to validate the design framework. Once the final prototype boots are constructed, they will be tested as described in Specific Aim 4.

3.1 Expected Outcomes



This thesis presents a process to design spacesuit components with improved fit and comfort. This process starts with understanding human-spacesuit interaction, then modeling dynamic body-shape changes at the area of interest, applying the body-shape changes to spacesuit design, and testing the resultant spacesuit component. This thesis outlines how this process has been applied to the spacesuit boot in the context of planetary walking. It is expected that the findings from the specific aims can be translatable to other spacesuit components of interest, which can follow a

similar process to improve fit and comfort. Future work will be required to assess how the findings from this thesis may need to be modified for applications to other spacesuit components.

Chapter 4

Specific Aim 1 : Challenges in Quantifying Heel-Lift during Spacesuit Gait

4.1 Introduction

Heel-lift is a subjectively reported fit issue in the MK III spacesuit, described as when the the Ground-based testing of the Mark III Advanced Space Suit Technology Demonstrator EVA Suit (MK III) has resulted in subjective reports of heel-lift, where the operator's heel lifts heel rises inside the boot before the boot's heel lifts heel lifts off the ground at heel-off[48]. Heel-lift can be represented as a lag between the operator's and spacesuit's heel-off times, and is an indicator of poor fit, leading to improper indexing of the ankle joint as the wearer goes to take a step. This improper fit; the statically-determined indexing between the operator's and spacesuit's ankle joints does not allow for dynamic alignment during heel-off. Since the foot freely moves within the boot during heel-lift, this could lead to injury through excessive contact or ankle joint overuse when taking a step. A better-fitting boot can help mitigate Foot contact injuries and discomfort were reported during simulated planetary walkback testing with prototype boot designs[32]. Designing a planetary spacesuit boot to mitigate heel-lift by captures the heel to prevent it from lifting during heel-off.

Designing such a boot, however, is difficult without knowing the frequency and magnitude of requires a quantitative understanding of its presence and magnitude. However, heel-lift ; the challenges of measuring has only been subjectively reported by spacesuit operators and has yet to be quantified through in-suit motion means that no direct measurements have been taken to date. Fineman et al. [48] used measurement techniques.

Various sensor technologies have been used to estimate relative motion between the spacesuit and operator, including pressure sensors[32], strain sensors[147], and inertial measurement units (IMUs) to measure [18, 48]. IMUs measure acceleration, angular velocity, and magnetic field; estimating orientation from these values. IMU Spacesuit applications include Fineman et al.'s[48] analysis of in-suit lower-torso kinematics lower-body angular velocities of subjects walking with the MK III spacesuit. IMUs measure the acceleration and orientation of the segment they're attached to, and have been successfully used in the biomechanics field to, and Bertrand et al.'s [18] estimation of in-suit upper-body joint angles during isolated joint motions. IMUs can detect heel-off points during gait[117, 50]. Heel-lift can be characterized as a lag between the operator's and spacesuit's [50, 117], and therefore may be able to identify heel-lift instances where spacesuit heel-off times; essentially, the operator experiences lags operator heel-off prior to the spacesuit doing so. IMUs were placed on both the operator's shank and the spacesuit's lower leg assembly (SLL), and it is assumed that the shank and SLL have a rigid connection their respective ankle joints. Therefore, the difference between the shank's and SLL's vertical position taken after the operator's heel-off time is the magnitude of heel-lift. While double-integrating an IMU's vertical acceleration signal is subject to integration drift,. However, IMUs can be subject to error in their orientation estimates due to the magnetic field inside the spacesuit environment, and integration drift when calculating linear displacement and velocity quantities from acceleration measurements. Digital filtering methods, zero-velocity (ZVUs), and zero-position updates (ZPUs) have been used in the biomechanics field to correct for integration drift at every step [46, 117]. However, IMUs are also subject to additional error in the spacesuit environment [18, 131, 132], bringing into question the feasibility of using these filtering methods on IMU data to detect heel-lift but these methods have not been evaluated in their ability to be robust against spacesuit-environment induced error.

Therefore, this work aims aimed to evaluate the ability of IMUs, ZVUs, and ZPUs to quantify the frequency and magnitude of heel-lift through the following objectives:

Detect heel-off times of both the spacesuit and the operator in the spacesuit. Heel-off times were detected using spacesuit lower leg and operator shank IMU data during suited walking

trials where IMUs are placed on the lower torso of both the spacesuit and operator. Evaluate the feasibility of zero-velocity and zero-position updates. Delayed spacesuit heel-off times compared to operator heel-off times were identified as potential occurrences of heel-lift. Then, ZVUs and ZPUs were evaluated for their ability to reduce integration drift and quantify the magnitude of reliability. Quantify the heel-lift magnitude.

4.2 Methods

4.2.1 Data Collection

Experimental data collected by Fineman et al.[48] was reanalyzed for this study. Three subjects walked in the MK III spacesuit with different padding levels at the hip and knee. Subject naming was kept consistent with Fineman et al.[48] for cross-reference of results, with subjects numbered 2-4 as Subject 1 did not complete all trials. Padding is frequently used to help index the operator's joints to the spacesuit joints. The subjects walked IMUs were placed on corresponding locations on the lower body of the spacesuit and operator, and different levels of internal padding were placed at the knee and hip (fig. 4.1). It is assumed that the IMUs' x-axis was aligned with the long-axis of the shank and SLL; this axis was considered the vertical task axis. Three subjects walked in the MK III spacesuit along a 10m walkway in each of four conditions: unsuited, MK III with no padding (configuration 0), MK III with one layer of padding, padding layer (configuration 1), and MK III with two layers of padding. Only the suited data was used in this analysis. All three padding layers (configuration 2). All subjects wore the same size MK III lower torso/lower body assembly, but Subject 3 wore a BOA-laced boot with fit adjustment at the tongue and heel, while other subjects wore a standard strap-laced boot. IMUs were placed in corresponding locations on the operator's and spacesuit's lower torso, while padding was placed in the pelvic and knee joints (fig. 4.1).

IMU vertical acceleration and pitch angle data from the operator's shank and the spacesuit's lower leg (SLL) was analyzed for this study. A with only tongue fit adjustment. This work only

analyzed a total of 216 trials were collected suited trials, each with data from the left and right sides of the operator and spacesuit, leaving yielding 432 datasets to analyze. For Data from Subject 2, Configuration's left leg during configuration 2, the left shank IMU dropped out for 11 trials, leaving 421 total datasets. For Subject 4, Configuration 0, Trials 1-12, the labels for the left and right IMUs seemed to be switched; the left SSL IMU was aligned with the right shank IMU and vice-versa was not included due to data loss from the IMU.

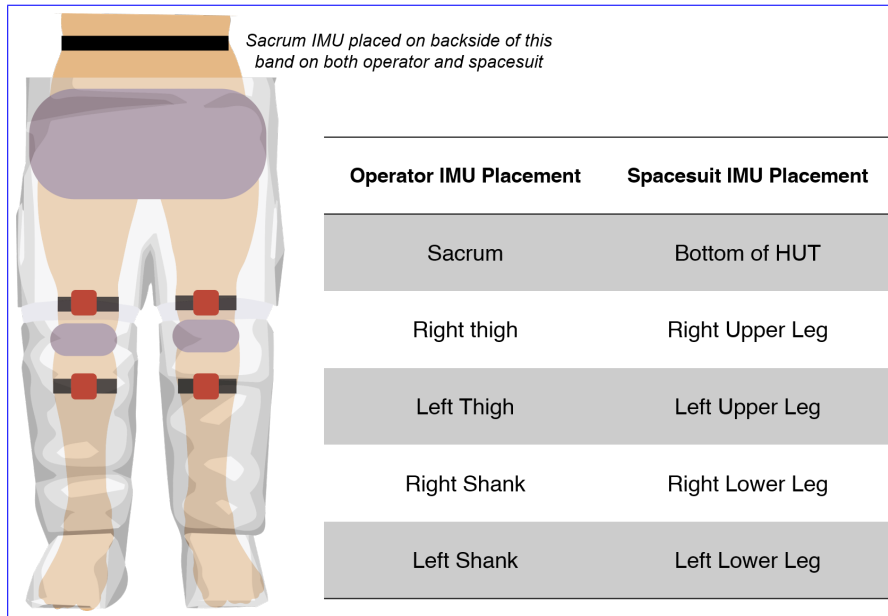


Figure 4.1: Location of IMUs (red squares, placed both the spacesuit and operator) and padding (gray). The sacrum IMU is placed on the back of the operator and spacesuit, where the upper-most black band is located, and is therefore out of view in this diagram. The table on the right outlines the IMUs corresponding locations between the operator and spacesuit.

4.2.2 Data Analysis

The IMUs' vertical acceleration along the shank and SLL's long axis, and the IMUs' pitch angle data were analyzed. It was assumed that the shank and SLL have a rigid connection to their respective ankle joints. Therefore, for these trials, the shank IMU was switched to the other side. Since it isn't known which IMU in particular was mislabeled, it is unclear if the new labels are right for these trials. However, since we are not analyzing our data by sides, this data was retained in the analysis. The difference between the shank's and SLL's vertical position taken after the operator's

heel-off time is the magnitude of heel-lift. Data analysis focused on isolating each individual step from the dataset, detecting heel-off points for the operator and spacesuit, and then implementing drift correction techniques to measure the vertical position of the shank and SLL.

Individual steps in the data for each trial was identified using detected peaks in the each trial were identified to begin analysis. The shank and SLL IMUs' pitch angles were smoothed using a 10-sample window moving average filter. Individual steps for each trial were then identified by detecting peaks in each IMU's pitch angle. These peaks are thought to correspond to, corresponding to the max posterior flexion/extension of the shank/SLL during the swing phase. The pitch angle is first normalized to it's first value in the time series for each trial. A moving average filter with a window of 10 samples, set through trial and error, was used to smooth the pitch angle. The minimum peak distance is set to 1.5s to ensure high-frequency peaks are not detected; this parameter was set based on the observed length of each step typically taking longer than 1.5s.

Since the first and last peaks of the trail may not be complete steps, they were not included in the analysis. Minimum peak prominence is set to 0.40 radians (23 degrees) to ensure that the first and last steps, which did not have complete swings, are not detected; peaks which corresponded to complete steps were observed to be closer to 0.60 radians (35 degrees). Each step is Each step was defined as the time between each step's max extension to the following step's max extension. An example of the step detection for a single trial is shown in fig. ??.

Once the locations of the peaks are detected, they are reshaped into an array which represents the start and end indices of each step. Since the peak detection is not a perfect algorithm, the number of steps detected in one trial for the SLL and shank might not be the same. Therefore, whichever IMU had the most amount of steps detected has its step times applied to the other IMU. This only occurred in 57 out of the total 421 datasets, when a step may not meet the minimum peak prominence threshold for either the shank/SLL IMU while meeting the threshold for the other, leading it to not be counted. The first and last peaks of the trial were removed from further analysis to ensure only complete steps were analyzed.

The foot-flat phase is the time duration within stance phase between toe-strike and heel-off. Foot-flat phase, where the foot is flat on the ground; detecting foot-flat phase allows for the detection of the between toe-strike and heel-off point, was identified to discriminate heel-off events. This phase is characterized by very low near-zero anterior-posterior acceleration; since the foot is flat on the ground, there is very little vertical movement of the shank[117]. Vertical acceleration data is preprocessed by first Raw shank and SLL IMUs' vertical acceleration data was preprocessed for foot-flat detection by de-trending to remove bias by removing the best straight-fit line from the data vector. A 30-sample window moving average filter with a window of 30 sample, equivalent to 0.23 seconds, is was then used to remove noise, within the range used for walking-speed estimation[24].

Discrete wavelet transforms (DWT) can be were used to detect gait events in from acceleration signals[71]. A 3-level discrete wavelet transform (DWT) is then DWT was applied to the preprocessed shank and SLL anterior-posterior acceleration signals. A Symlets 2 wavelet (**sym2**) is was then used as the mother wavelet for the transform, due to its high performance in detecting initial-contact and final-contact points during stance phase[71]. After transforming to wavelet space, a threshold is was applied where values below 2% of the maximum wavelet coefficient are were set to zero. The wavelet coefficients are were then reconstructed back into a signal and then used to detect foot-flat phase.

Foot-flat phase is was detected by looking for the zero regions in the shank and SLL's acceleration's derivative [92] derivative10. A threshold of $0.01m/s^2$ $0.01m/s^3$ was set to account for small amounts of noise in the DWT signal. Acceleration points within this threshold were identified as zero-acceleration points. Zero-acceleration points less than 3-samples long are were removed, since foot-flat phase is expected to be much longer. The end of Fig. 3 shows an example of isolating foot-flat phase is heel-off, while the beginning is toe-strike. An example of detecting foot-flat phase is shown in fig. ?? from DWT transformed signals. The difference in heel-off times between the shank and SLL can be heel-off times was used to detect instances of heel-lift; a positive value would mean the operator experience corresponds to operator heel-off before the spacesuit, which

would indicate prior to spacesuit heel-off, suggesting heel-lift. Quantifying these differences across all datasets can help determine the frequency of occurrence of heel-lift.

The heel-off detection was not perfect. In some cases, it failed to properly detect heel-off for the operator or spacesuit with the parameters provided. Heel-off lag times <-0.2s and >0.2s were manually inspected, and if the detection times were incorrect visually noted to be misaligned with the zero-acceleration period, these steps were taken out of the analysis. Only removed from analysis. A total of 32 out of a total of 1381 steps met this criteria for removal.

Double-integrating the acceleration signal to calculate IMU position is. The vertical acceleration signals from the IMUs are subject to integration drift when converted into positional estimates using double-integration. The raw vertical acceleration signals were preprocessed by a 10 Hz low-pass filter to remove high-frequency noise[12]. Zero-velocity (ZVU) and zero-position updates (ZPU) are used to reduce integration drift and improve the accuracy of the positional estimate of the shank and SLL. The vertical acceleration signal is preprocessed by first detrending and then low-pass filtering at 10 Hz to remove high-frequency noise [12]. ZVUs rely on the fact that during gait, the vertical velocity of the shank or SLL will be zero during It is assumed that the shank and SLL's vertical velocities were zero just prior to heel-off, when the operator and spacesuit are in stance phase. Therefore, this known fact can be used to correct the signal to zero during known stance phases. Using this assumption, a linear correction is applied retroactively for each step between heel-off times. At the identified heel-off times, the vertical velocity is set to 0 was set to zero, and the vertical velocity after during the step prior to heel-off is was subtracted by the velocity reported at heel-off weighted based on the distance from the heel-off timepoint using formula. The following step's vertical velocity was then corrected to the heel-off velocity. This process is summarized in eq. 4.1, originally presented by Feliz et al. 2009 [46]:

$$v'_{x,i} = v_{x,i} - v_{HO} * \frac{t_i - t_{TS}}{t_{HO} - t_{TS}} \quad (4.1)$$

where at timestep i after heel-off, $v'_{x,i}$ is the corrected velocity, $v_{x,i}$ is the original velocity, t_i is time, TS is the next toe strike v_{HO} is the velocity at heel-off, t_{HO} is the previous step's heel-off

timepoint, and ~~HO is the next t_{HO} is the current step's~~ heel-off timepoint. ~~An example of how ZVUs reduce drift is shown in figure ??.~~ Integrating the corrected velocity signal to obtain the IMU's position ~~will can~~ similarly be subject to integration drift. It ~~is was~~ assumed during stance phase that both the operator's foot and the spacesuit boot are flat on the ground and therefore the shank and SLL are not moving vertically. ZPUs can use this ~~known fact~~ to correct for drift by zeroing the position estimate for both the SLL and shank at heel-off. ~~Since the The~~ shank and SLL ~~are were~~ assumed to be rigidly connected to their respective ankle joints, ~~taking the difference in shank and SLL vertical position after~~. Heel-lift magnitude can be then defined as ~~the vertical displacement difference between the shank and the SLL at the SLL's heel-off will give an estimate of heel-lift magnitude~~ timepoint.

~~Since drift Drift~~ is not completely eliminated with the outlined methods, ~~bounds need to be established where we can take the positional difference~~. An upper bound was calculated to inform ~~the time limit past the heel-off correction point where heel-lift magnitude can be quantified~~ with confidence that the ~~difference magnitude~~ is not largely due to ~~the~~ drift. While drift is not ~~exactly~~ a linear process, an assumption was made that calculating the drift magnitude between two known ~~time points~~ ~~timepoints~~, and dividing ~~it~~ by the elapsed time, would be a reasonable approximation to quantify how drift ~~accumulates over time in this scenario~~ accumulation. During stance phase, it ~~'s was~~ expected that both the SLL and shank ~~will would~~ have the same vertical position at toe-strike and heel-off. During swing phase, it ~~is was~~ expected that both IMUs ~~will would~~ return to the same vertical position after each step. Drift magnitude was calculated for each detected step by subtracting the post-ZVU/ZPU position values at the beginning and end of stance phase and swing phase from each other, and then dividing by time of each phase, to ~~get a average~~ drift rate. This rate represents the amount the IMU's positional estimate has drifted over each phase following correction from ZVU/ZPUs, when it is expected to return to ~~0 zero~~. Analyzing the distribution drift rates across all trials ~~will allow for a allowed for the upper~~ time-bound to be defined where drift magnitude is minimal and can ensure accuracy in the calculated position values.

4.3 Results

~~Median drift rates following ZVU/ZPUs~~ Figure 4.2 shows the distribution of heel-off lag measurements across conditions, subjects, and sides. Subject 2 experienced spacesuit-delayed heel-off in 97 (20 left, 77 right) out of 382 (151 left, 231 right) total steps. Subject 3 experienced spacesuit-delayed heel-off in 305 (155 left, 150 right) out of 410 (204 left, 206 right) total steps. Subject 4 experienced spacesuit-delayed heel-off in 45 (21 left, 24 right) steps, and operator-delayed heel-off in 226 (87 left, 139 right) steps out of 481 (237 left, 244 right) total steps.

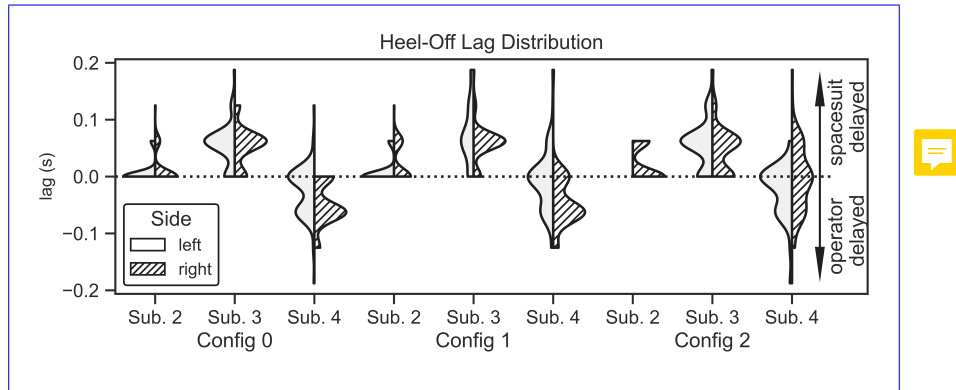


Figure 4.2: Heel-off lag distributions between all subjects and configurations, with discrete heel-off lag measurements being represented as black dots. Positive lag values are indicative of spacesuit-delayed heel-off, while negative lag values are indicative of operator-delayed heel-off

~~Mean drift rates after correction~~ for both the SLL and shank IMUs are presented in table 4.1. ~~The SLL showed much higher drift rates than the shank, which may be due to that IMU being subject to the spacesuit's magnetic field disturbances. The SLL drift rate during stance phase, where the heel-lift positional difference is taken following heel-off, therefore defines an upper confidence limit of 0.04 s~~ An upper confidence bound of 0.03 s (1/32 cm/s) was found to take a heel-lift measurement with an accuracy of ~~1cm, based on the mean shank IMU swing phase. Average step duration across all trials was 1.6 ± 0.2 s; therefore drift accumulated over 1 cm (1/26.33 cm/s)~~ on average within 2% of the step duration.

Table 4.1: Drift rate estimations (mean +/- std dev) of raw, filtered, and ZVU/ZPU positional estimates for IMUs mounted on the spacesuit leg assembly and shank



IMU	Phase	IMU	Stance Phase Median Drift Rate Raw	Swing Phase Median Drift Rate ZVU/ZPU
Shank	Stance	Shank	$9.48 \pm 43 \pm 63$ cm/s	$14.15 \pm 5 \pm 6$ cm/s SLL
		SLL	$26.33 \pm 241 \pm 130$ cm/s	$27.48 \pm 16 \pm 11$ cm/s
Swing		Shank	67 ± 59 cm/s	32 ± 16 cm/s
		SLL	265 ± 103 cm/s	66 ± 40 cm/s

Since 0.04 seconds is a very small amount of time in the context of gait events, it was decided to not record any heel-lift magnitudes as they would be much less than the 1 cm accuracy assumption used to derive the limit. Measurements taken after this point may not be trustworthy. Heel-lift magnitude was not calculated due to the presence of accumulating drift, operator-delayed heel-off lag noted in Subject 4, and high drift rates following correction resulting in a low upper time-bound for calculating heel-lift magnitude after heel-off.

Heel-off lag was calculated for all retained datasets. Figure fig. ?? shows the distribution of

4.4 Summary

This study aimed to evaluate the use of IMUs with ZVUs and ZPUs to quantify heel-lift in spacesuit gait. Methods were demonstrated to determine heel-off lag measurements across all conditions and subjects. Only Subject 4 experienced “negative” points on the shank and SLL IMU; where a lag in the spacesuit’s heel-off lag, where the spacesuit experiences point compared to the operator’s heel-off before the operator. point would suggest heel-lift. All subjects experienced varying amounts of spacesuit-delayed heel-off across conditions, with no noticeable effect from padding. Subjects 2 and 3 experienced only “positive” 4 had more counts of spacesuit-delayed heel-off lag, which would suggest that these subjects experienced heel-lift. Example steps for these figures on their right compared to their left side (Subject 2: 33% vs. 13%, Subject 4: 57% vs. 37%).

suggesting a looser boot fit on their right side. Heel-lift was subjectively reported only by subject 26. Only subject 4 experienced operator-delayed heel-off. Examples of both operator-delayed and spacesuit-delayed heel-off are shown in ~~an example step is shown in fig. ??4.3.~~

“Negative”

Operator-delayed heel-off ~~lag~~ is theoretically impossible ~~with the assumptions made in this study:~~ when the spacesuit ~~experiences~~ ‘s boot rises during the spacesuit’s heel-off ~~timepoint~~, it will ~~also~~ push on the operator’s heel, ~~causing it to experience~~ ~~registering a simultaneous operator~~ heel-off ~~as well.~~ However, the assumption that the SLL is rigidly connected to the spacesuit’s ankle was previously stated. Since the SLL is made of soft goods, it ~~timepoint~~. The SLL’s soft goods can expand and contract in length due to internal pressure forces or interactions from the knee or femur. Therefore, [65]. Longitudinal restraint straps are employed in spacesuit design to balance tension and pressurization forces at joints, but are not usually integrated along non-bending components such as the SLL [65]. Therefore, the SLL may be expanding in length for Subject 4 at heel-off, causing the IMU mounted on the SLL to register a positive acceleration and therefore the illusion that the spacesuit experiences heel-off before the operator. This may not be initial assumption that the SLL is rigidly connected to the boot is broken. False-positive vertical accelerations due to segment lengthening are not a concern for the shank-mounted IMU, as the shank ~~is rigidly connected to the ankle and it is assumed that~~ and ankle are rigidly connected and the IMUs are assumed to be rigidly strapped to their segments. It is also important to note that Subject While soft-tissue artifacts may be present, they are likely of a much smaller magnitude. The SLL may be expanding in length for Subject 4 had larger lower-torso anthropometry than Subjects 2 or 3, which may cause greater leg lengthening.

~~Zoomed-in view of one example step’s foot-flat phase showing “negative” A and “positive” heel-off lag B. The shaded regions represent the detected foot-flat regions for the operator (blue) and spacesuit (red); an increase in vertical acceleration for the shank IMU (blue) prior to the SLL IMU (red) is “positive” heel-off lag, suggesting heel-lift B, and vice-versa A.~~

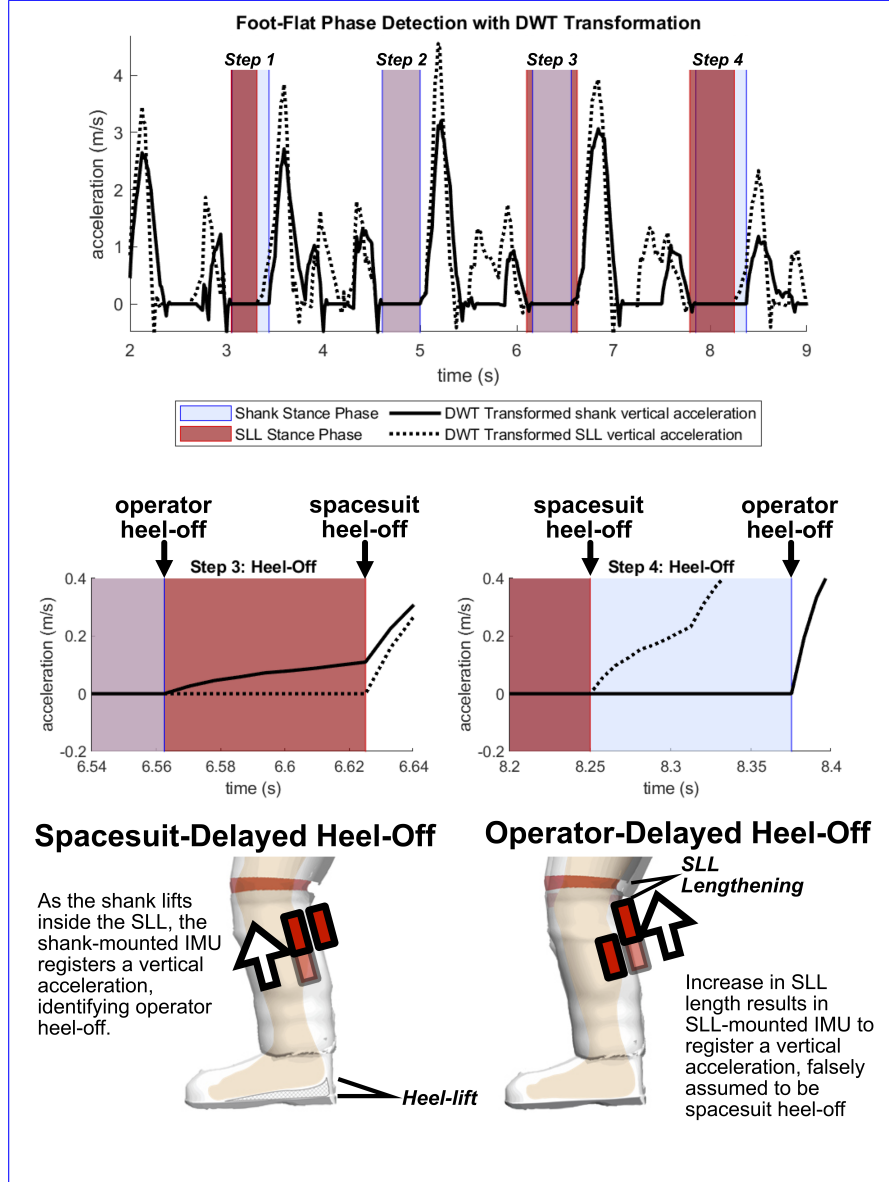


Figure 4.3: (Top): DWT IMU vertical acceleration data for shank and SLL. Shaded regions represent the detected foot-flat phases of zero-acceleration regions for each step. (Middle) Zoomed-in view of the foot-flat phase for two steps, with annotated spacesuit and operator heel-off points. When the shank IMU registers a vertical acceleration in foot-flat phase prior to the SLL IMU (middle-left), this could suggest heel-lift (bottom-left). When the SLL IMU registers a vertical acceleration in foot-flat phase prior to the shank IMU, this would ordinarily suggest that the SLL experiences heel-off prior to the operator (middle-right). However, there may be pressure forces which allow the SLL to extend, registering a vertical acceleration for the SLL-mounted IMU and falsely suggesting that the spacesuit is experiencing heel-off (bottom-right).

The soft-goods design of the SLL does not allow for the accurate detection of at heel-off^{lag}
between the shank and SLL since it breaks the assumption that the SLL is rigidly connected to

the ankle. In addition, ZVUs/ZPUs did not reduce integration drift enough to warrant using IMUs to measure heel-lift magnitude.

While the results of this study may not directly translatable to boot design, they do show that the causing the IMU mounted on the SLL may be changing length during to register a positive acceleration prior to the operator. Subject 4 wore the same size suit lower assembly as other subjects but had larger crotch and knee heights. As such, there would be more room in the lower leg assembly for the soft goods to expand, providing a possible explanation for why only Subject 4 experienced operator-delayed heel-off. This can influence the forces acting on the boot.

A tighter boot fit, where the heel stays indexed in the boot, as well as the shank and knee of the operator allows the operator to overcome expansion forces that push the SLL down, resulting in the SLL extending upwards and registering as operator-delayed heel-off. In contrast, loose boot fit will not allow the operator to overcome these forces, and will push the boot down, keeping it on the ground and registering as spacesuit-delayed heel-off. Fineman et al [48] suggested that relative coordination of the lower torso may be affected by boot summarized that Subject 4 had synchronous motion of the shank and SLL between heel-off and toe-off; Subjects 2 and 3 had motion driven by the suit, suggesting heel-lift. Data from this study similarly suggests that Subjects 2 and 3 experienced more instances of spacesuit-delayed heel-off than Subject 4. Therefore, Subject 4 may have had a tighter boot fit as indicated by operator-delayed heel-off, and operator-delayed heel-off may serve as an indicator for tighter boot fit issues, which may suggest that boot itself may be contributing to the forces extending the SLL.

Findings from this study suggest that current IMU technology and drift correction techniques alone may not be appropriate for quantifying the presence and magnitude of heel-lift in the space-suit environment. Drift evaluation showed that the SLL-mounted IMUs had higher drift rates than the shank-mounted IMU. Potential sources of increased drift could be effects from the SLL segment's soft-goods expansion and contraction [48, 65], resulting in different frequency components compared to the shank's movement. While ZVUs and ZPUs did substantially reduce drift in stance and swing phase, drift was still present in this study. Heel-lift magnitude measurements

could not be taken with confidence that magnitude differences would be due to heel-lift. Future work may incorporate the use of contact sensors or pressure insoles in the spacesuit boot to check for heel-contact, along with optical capture of the spacesuit boot's kinematics to accurately detect heel-off points. Such techniques can be used to augment the presented heel-off detection for the operator inside the spacesuit. Improvements explore the extent of soft-goods expansion on spacesuit kinematics analysis, which may affect positional estimates from optical motion capture. IMUs have been shown to measure spacesuit angular kinematics with a root-mean-squared error of 4.8-5.8 degrees[18] and were used to characterize relative angular coordination within the suit[48], but have not been evaluated for accuracy in spacesuit positional estimates as conducted in this study. Suit components should only expand longitudinally, and should therefore not affect angular estimates[65]. Other sensing modalities or improvements to IMU mounting on the spacesuit or characterization of the SLL leg lengthening may also decrease the effect of spacesuit pressure forces may be more appropriate in quantifying the vertical displacement that defines heel-lift. Updated sensor technology can also characterize the spacesuit leg lengthening effect, allowing it to be isolated from the IMU's signal. Contact sensors and pressure insoles will be evaluated for testing in Specific Aim 4.

Currently, all analysis is complete with this work. This work is currently in preparation as a technical note to be submitted for peer-review Characterization of in-suit motion will be required to develop comfortable and safe planetary EVA spacesuits. This study highlighted the challenges of using IMUs to measure in-suit motion, concluding that IMUs may not be appropriate for measuring in-suit displacement at the magnitude expected during heel-lift. The primary assumption that the SLL was rigidly connected to the ankle joint was not supported; the observed operator-delayed heel-off suggests that the SLL is vertically extending during gait. Fineman et al [48] hypothesized that lower-body relative coordination may be affected by boot fit issues. Future work can characterize SLL extension throughout the gait cycle, further understanding the forces acting on the SLL due to fit. Sensor technologies can also be evaluated to study heel-lift, such as resistive or capacitive force sensors mounted under the heel to directly measure heel contact, or

strain sensors mounted between the human and suit to measure displacement. Such methods can be used to evaluate spacesuit components susceptible to injury, such as the gloves or upper torso[32]. IMUs can be mounted directly to the boot to isolate ankle kinematics from SLL lengthening and accurately detect heel-off points using the presented methods and assumptions. Force plates can directly identify spacesuit heel-off points, therefore not requiring suit-mounted IMUs. Developing and evaluating various in-suit motion measurement techniques will help improve spacesuit design and fit, reducing the risk of injury and ensuring mission success for future planetary EVAs.



Chapter 5

Specific Aim 2: Predictively model dynamic changes in foot morphology during gait

5.1 Introduction

Designing a new spacesuit boot to be more comfortable and not be subject to fit issues like heel-lift, requires a thorough understanding of foot shape. However, foot shape is known to be highly variable throughout the population, including by sex [156, 83, 84], age [141], and weight [115]. This variability is often not captured in terrestrial footwear sizing, as current fitting standards only use foot length, foot width, and arch length to fit to standardized shoe sizes [13]. Furthermore, terrestrial footwear is commonly designed around lasts, shoe molds that are sized and shaped by each manufacturer with no common standard. This leads to variability in footwear shapes and sizes [72, 148], making it hard for consumers to find a proper fit and resulting in users having to wear ill-fitting footwear with suboptimal comfort. ~~Foot problems and resultant pain have been reported due to poor fit in coal mining boots [39]~~ and being at risk of occupational injury during ambulation [39]. Footwear fit and comfort has shown benefits in increasing biomechanical performance [116], reducing the risk of movement-related injury [99], and is often the number one factor for consumers to select footwear [93]. Therefore, the issue of footwear fit and comfort is not just limited to spacesuit boots, both terrestrial footwear and spacesuit boots should account for the wide variety of foot shapes to improve fit.

In addition to foot shape variability in the population, the foot also changes shape while being loaded during gait. The current methodology of designing terrestrial footwear uses static

lasts, assuming that the foot consists of rigid segments. Assumptions of rigid foot segments during foot loading have shown inaccuracies in estimation of ankle joint mechanics [159, 76],~~suggesting intra-foot motion as the foot~~. Evidence has been presented on articular motion within the foot as it is loaded [86, 155].~~Evidence suggests~~, and that foot loading affects linear foot measurements, such as when transitioning from sitting to standing [157, 106] or during the stance phase of gait [81, 14, 60]. The dynamically changing measurements suggest morphological changes occurring, all of which may not be captured in static linear and circumferential measurements. Thus, footwear should also be designed to account for these dynamic foot shape changes.

Statistical shape models (SSMs) can explain morphological differences across populations and during motion by identifying shape modes which account for variance from the mean shape. These have been developed for whole-body digital human modeling applications to study population and individual variance in body shape [4, 11, 120, 109, 110]. Parametric SSMs are extensions which use correlations between subject anthropometric data and SSM deformations to help predict body shape for new individuals in the population [109, 110]. The ABF at NASA developed parametric SSMs to characterize shoulder shape deformation across the shoulder's range-of-motion, predicting shape as a function of shoulder orientation, to validate HUT design [78, 77]. However, the technology used to capture the body scans for this SSM could not capture the dynamic natural motion of the shoulder; subjects had to pose their shoulder at specific orientations while a scan was taken.

~~SSMs have recently been applied to characterize static foot shape across a population [35]~~
~~and recognize foot-shape deviations [133].~~ The aforementioned efforts to capture foot measurement changes over the gait cycle did capture 4D foot images ~~at high framerates~~[14, 60], but these efforts ~~were not translated into a SSM focused on extracting changes in foot measurements and not volumetric predictions of foot shape.~~ SSMs have recently been applied to characterize static foot shape across a population [35] and recognize foot-shape deviations [133, 129], but these efforts ~~were not predictive~~. Previously developed systems were based on a catwalk, requiring subjects to correctly hit the scanning area for a successful data capture, which may not be representative of natural cadence. However, the systems used to capture 4D foot shape are very expensive and cannot

be used around a treadmill, which allows for subjects to fall into natural gait. ~~No~~Therefore, no SSMs have been developed from previous capture of 4D foot scans to predict dynamic foot shape.

Therefore, the objectives of this specific aim are:

- Develop a low-cost 4D scanning system capable of capturing foot shape around a treadmill
- Create a predictive model of foot shape changes across the dorsal surface during stance phase
- Identify specific areas of the foot that change shape during stance phase
- Correlate changes in foot shape across large-scale population foot measurements

5.2 DynaMo: Dynamic Body Shape Capture with Intel RealSense Cameras

A low-cost 4D scanning system, DynaMo, was developed to capture dynamic foot shape during gait. Human body shape can be captured with a variety of methodologies, including laser lines, structured light, photogrammetry, and millimeter waves [38]. However, these technologies require expensive modules and have limited ability to capture dynamic changes in body shape. Motion capture with specific markers is commonly done through camera-based motion tracking [153] These systems for marker tracking are often cost prohibitive and unable to capture surface morphology.

Therefore, the DynaMo software library was developed to use multiple commercial depth cameras, the Intel RealSense DXX Depth Cameras (Intel, Santa Clara CA), retailing between \$150-\$200, to capture dynamic body shape changes. The Intel RealSense Depth cameras use two stereo image sensors along with a structured light projector to capture depth maps at 90 frames-per-second; each pixel in a depth map records the distance from the camera to the world. DynaMo includes functions to calibrate a capture volume, using a checkerboard to identify a common origin between multiple depth cameras (fig. 5.1). DynaMo calculates a common point cloud from the depth maps of all the connected cameras, outputting a point cloud for every frame captured by all connected cameras (fig. 5.2). Functions were also developed to track the position of reflective markers in the scene. The development of DynaMo was published in a journal paper [20].

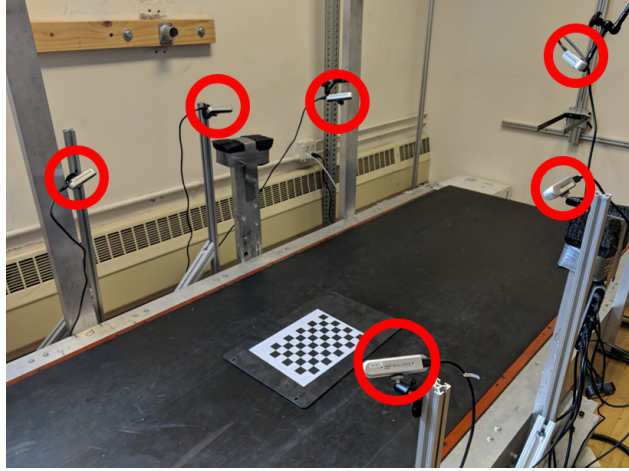


Figure 5.1: Capture setup of 6 Intel RealSense D415 Depth Cameras (circled in red) placed around a treadmill. The checkerboard shown was used to calibrate the cameras using the DynaMo package.

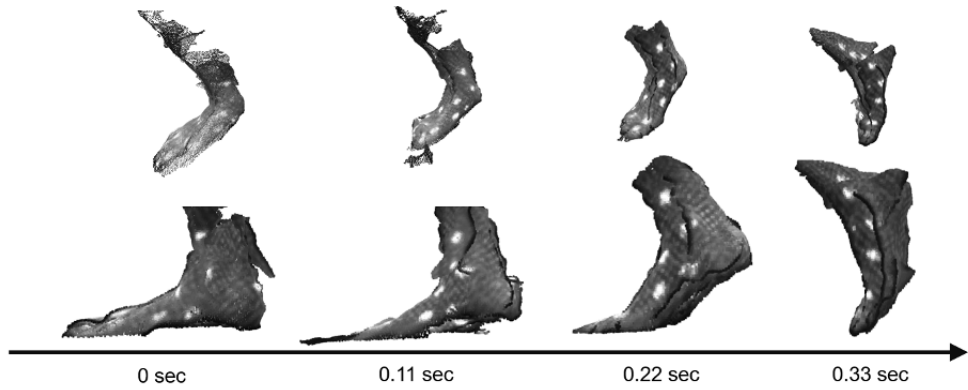


Figure 5.2: Sample frames, shown in 10 frame intervals (bottom), collected by DynaMo showing dynamic shape capture of the foot (top) at 90 frames-per-second, and the capture of reflective markers on the foot shown as white dots

A post-hoc accuracy analysis was conducted on the DynaMo software and Intel RealSense D415 cameras. A shoe last with a corresponding 3D digital model was placed in the capture volume between all cameras, and scanned 10 times. The last was removed and replaced in the volume between each scan. Root-mean-squared error was then calculated between each resulting 3D scan, and the 3D digital model, and was found to be 2.5 /pm 0.5 mm.

5.3 Development of a Predictive Dynamic Foot Shape Model from Statistical Shape Modeling

The ~~development of the~~ DynaMo software [20] allowed for a capturing of foot shape to develop a parametric SSM. This system captures foot morphology changes during loading and unloading on the foot's dorsal surface, but does not capture of the foot's plantar surface. A parametric SSM was developed which can characterize and predict dynamic foot morphology at specific points during stance phase across the subject population.

5.3.1 Methods

5.3.1.1 Subjects

A total of 30 healthy subjects (15 men and 15 women, ages 23.1 ± 3.7) participated in this study. Subjects were recruited in a stratified sample into one of six groups (5 subjects per group) to maximize variance in population foot length. Height was used as the grouping factor since height is well correlated to foot length [56]. The general population may not know offhand their exact foot length, and shoe size varies by manufacturer and does not correspond directly to foot length [72, 148]. Groups consisted of 5th-35th, 35th-65th, and 65th-95th height percentiles for each sex. Height percentile values were taken from the ANSUR II survey [57]~~and converted to imperial units as it was expected most subjects would report their height in imperial units.~~

Population recruitment groups are summarized in *tbl. 5.1.*

Table 5.1: Enrollment groups based on reported height. 5 subjects were enrolled in each group

Sex <u>Sex</u>	5th-35th percentile Height centile Height	35th-65th per- centile Height	65th-95th percentile Height
Female <u>Female</u>	4'11"-5'3"	5'3"-5'5"	5'5"-5'8" Male
Male <u>Male</u>	5'4"-5'8"	5'8"-5'11"	5'11"-6'2"

Sex <u>Sex</u>	5th-35th percentile Height	35th-65th per-	65th-95th percentile Height
	centile Height		

Prior to recruitment, subjects completed a prescreening survey to ensure they were adequately healthy by the American College of Sports Medicine guidelines [121], and between the ages of 18-65. Subjects provided their sex and height, and were only enrolled in the study if their population group was not fully enrolled.

5.3.1.2 Experimental Procedures

The experimental protocol was approved by the University of Colorado Institutional Review Board. Procedures were explained to each subject and written consent was obtained prior to participation. Subjects' height and weight were recorded with a tape measure and scale, respectively. Subjects' foot length, foot width, and arch length were measured with a Brannock device (The Brannock Device Company, Liverpool, NY) [13]. Both foot length and arch length were measured in centimeters. Foot width was measured as an ordinal size (e.g. A, B, C, D, E), and then converted to a linear measurement in centimeters (The Brannock Device Company, Liverpool, NY).

Six Intel RealSense D415 Depth Cameras (Intel, Santa Clara, CA) were placed and calibrated around a custom-built level treadmill in the University of Colorado Boulder Locomotion Laboratory, as shown in fig. 5.1. The treadmill was set to an average walking pace of 1.4 m/s [23]. Reflective markers were placed on the subject's right foot and a black sock over their left foot to aid in right foot identification. Subjects first walked for one minute to warm-up and fall into a natural cadence. The operator then collected 10 seconds of data to capture approximately 10 steps. The data were reviewed to ensure the subject stayed in frame from heel-strike to toe-off during capture. If needed, the subject's placement was shifted and data was collected again, up to two times.

5.3.1.3 Data Processing

Figure 5.3 provides an overview of the data processing workflow; all steps are summarized in the paragraphs below.

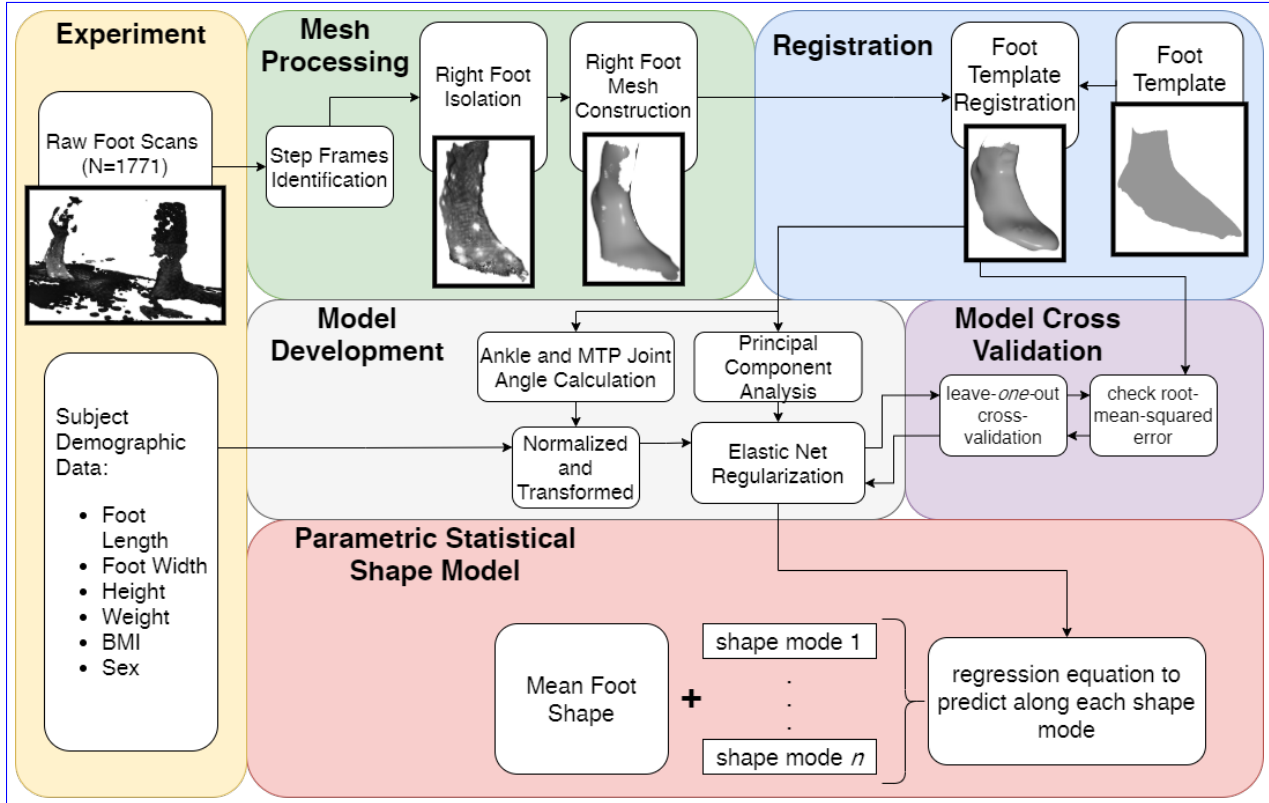


Figure 5.3: Flowchart of processing steps for statistical shape model creation

For each subject, a single candidate heel-strike to toe-off event was manually identified across all captures by taking into account point cloud quality due to the high computational power required to process all heel-strike to toe-off events. Events with holes greater than 1cm that appeared across more than one frame were rejected. The depth images captured by each depth camera were processed into point clouds using the DynaMo package [20]. From each point cloud, the right foot was isolated and transformed into a triangle mesh [123, 51, 17, 161]. Since every depth image was captured independently by the cameras, the amount and location of points which represented the foot were not consistent. ~~In addition, the captured data may have holes in the surface representing the foot.~~ Registration of all scans to a common template represents every scan by an equal number of

points, and ensures any missing points not meeting the rejection criteria are properly interpolated. The right foot meshes were then iteratively registered using a three-step fitting process to an averaged high-quality static template scan, provided by Dr. Matthew Reed from the University of Michigan Transportation Research Institute [118]. First scans were roughly aligned using a point-to-plane iterative-closest-point algorithm [34], implemented in Open3D [161]. Next, the radial-basis function fitting algorithm from the GIAS2 software package [160] was run twice using a thin-plate spline to approximate the foot surface [109, 78]. The mid-stance scan from each subject was registered first to the template, and then the registration process was run both forwards towards toe-off and backwards towards heel-strike, on a scan-by-scan basis, using the previously registered scan as a template for the next scan. Accuracy was checked by comparing registered scans with the processed scans by finding corresponding points between both, and calculating the root-mean-squared error (RMSE) between the corresponding points.

Anatomical landmarks can be reliably were approximated from the registered scans using the foot features of the registration template [142]. The first metatarsal head, fifth metatarsal head, and second toe landmarks were used to align all scans to be centered at the second metatarsal head, with the forward axis pointing towards the second toe. Landmarks around the metatarsalphalangeal (MTP) joint and ankle joint were used to calculate ankle, MTP, and foot kinematics for each subject's scans with respect to the joint angles at the subject's mid-stance scan. Relevant joint angles include dorsi/plantarflexion, ankle inversion/eversion, ankle internal/external rotation, MTP dorsi/plantarflexion, foot inversion/eversion, and foot internal/external rotation angles.

5.3.1.4 Model Construction

Principal component (PC) analysis is a dimensionality-reduction method commonly in constructing SSMs [119, 109, 35, 133]. The first PC represents an axis containing the largest variance in the dataset, and each subsequent PC describes the largest variance orthogonal to the previous component's axis. Therefore, PCs allow for a new, smaller set of orthogonal variables to be defined which represent the variance in the dataset.

Let N equal the number of total scans in the dataset, and $n = 29873$ equal the number of vertices in each registered scan. The scikit-learn module [112] was used to incrementally calculate the maximum N PCs which represent the dataset. Each scan in the dataset is represented in the PC model with N PC scores. All PC scores are centered around 0, which represents the mean foot scan of the dataset containing all subjects. Each PC represents a shape mode in the SSM, where each score represents a deviation from the mean foot along the shape mode axis. The resultant PC model can be used to inverse transform a vector of length N PC scores into a 29873×3 vector, which represents the location of the vertices in the foot shape. Not all PCs were retained in the model since the first few PCs explain a majority of the variance, while additional PCs may be accounting for noise.

Subject demographic data and calculated joint angles were incorporated into the SSM by developing multivariate linear regression models based on these features. This was used to predict each PC score, which can then be inverse-transformed into a foot shape. Subject demographic data and joint angles were independently unit normalized and power-transformed across the whole dataset to aid in regression development [158]. An elastic net regularization algorithm [162] was run for each multivariate regression to calculate normalized feature coefficients for each PC score's regression. Two different sets of predictors were created, one with all subject demographic data and calculated joint angles, and one with the highly cross-correlated predictors of arch length, body-mass index, and height were removed. Six potential models were built as combinations between the number of PCs predicted which explained 95%, 98%, and 99.7% of the variance, and the two predictor sets.

5.3.1.5 Model Validation

All six models were validated for performance using leave-one-out cross-validation, where scans from each subject were set as the validation set, and models were trained on the remaining dataset. Model performance during validation was quantified with the root mean squared error (RMSE) and Hausdorff distances of the predicted foot shape to the corresponding registered scan. A two-way RMANOVA analysis was run on the error distributions to test the effect of constructing

a predictor with the different number of PCs, and between using the two variable sets. The chosen model was retrained on the whole dataset before being analyzed.

5.3.2 Results

A total of 1771 scans were analyzed across all 30 subjects. The average number of scans collected for each subject's stance phase was 59 ± 3.7 , with a range of 52-69 scans due to inter-individual differences in stride length. Figure 5.4 shows a set of raw and registered scans from one subject. All processed scans were registered to the template with a ~~median registration accuracy~~
mean registration RMSE of 1.0 ± 0.6 mm, and a mean Hausdorff distance of 25.5 ± 13.4 mm.

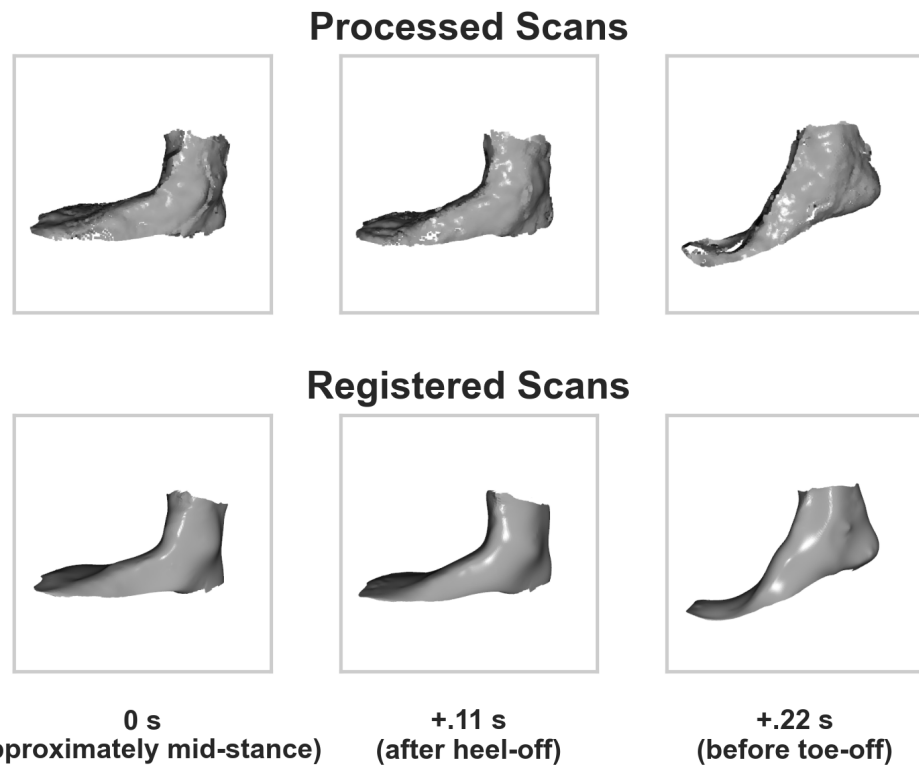


Figure 5.4: Processed and registered scans of one subject during heel-off, shown 10 frames (0.11 seconds) apart.

The PCA analysis of all registered scans found the first 8 PCs to represent approximately 95% of the variance, the first 27 PCs to represent approximately 98% of the variance, and the first 105 PCs to represent approximately 99.7% of the variance. ~~Figure 5.5 (Fig. 5.5)~~ shows the distri-

bution of cross-validation RMSEs ~~and Hausdorff distances~~ for each of the six ~~elastic net regression~~ models tested. ~~RMSE-Aligned-Rank Transform [154] was used to compare models as error~~ distributions did not meet assumptions for normality, ~~but RMANOVA was still used to compare models due to its resiliency to deviations from normality.~~ A significant difference was found. Significant differences were found in RMSE and Hausdorff distances between predicting different numbers of PCs (~~RMSE: F=1595.07037, p<0.001; Hausdorff distances: F=4577, p<0.001~~), predicting between the two variable sets (~~RMSE: F=81.6, p<0.001~~ $F=6.4, p=0.012$; ~~Hausdorff distances: F=4.4, p=0.036~~), and ~~the interaction between both factors (for the interaction (RMSE: F=213.7, p<0.001)~~. Significant differences were found between all three levels of the predicted number of PCs ($p\text{-adj}<0.001$) with a Tukey post-hoc HSD test. No significant difference was found between the two variable sets ($p\text{-adj}3.0, p=0.42$). 0.05 ; Hausdorff distance: $F=5.3, p=0.005$). An ART-C post-hoc test [43] with Bonferroni correction found significant differences between all but one pair of models; detailed results are presented in supplementary information. Therefore, the model predicting 8 PCs with the selected variable set was chosen for its simplicity and performance.

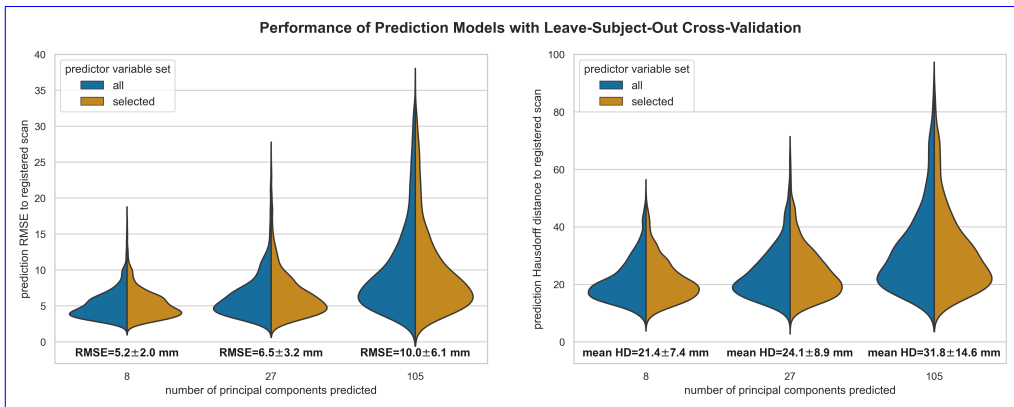


Figure 5.5: Distribution of mean root-mean-square (RMSE) error and mean Hausdorff distance (HD) across the various prediction models leave-subject-out cross-validation results. Model error values and standard deviation are shown below each distribution

Each retained PC is a shape mode~~in the model~~. ~~Figure 5.6. (Fig. 5.6)~~ shows the chosen model's normalized regression coefficient values for each shape mode. The coefficients for the sex predictor are not shown as they were ~~e~~calculated~~predicted~~ to be zero for every shape mode.

(Fig. 5.3.2) shows each shape mode's axis represented on the mean foot, highlighting which areas of the foot are affected by deformations in each shape mode. (Fig. 5.3.2) shows the ± 2 standard deviations of deformation along each shape mode overlaid on the mean foot. Supplementary information includes correlation between predictors, ratio of total variance each retained PC accounts for, and a link to an interactive web tool to visualize the model. All data from this project is available online.

Normalized Regression Coefficients per Shape Mode

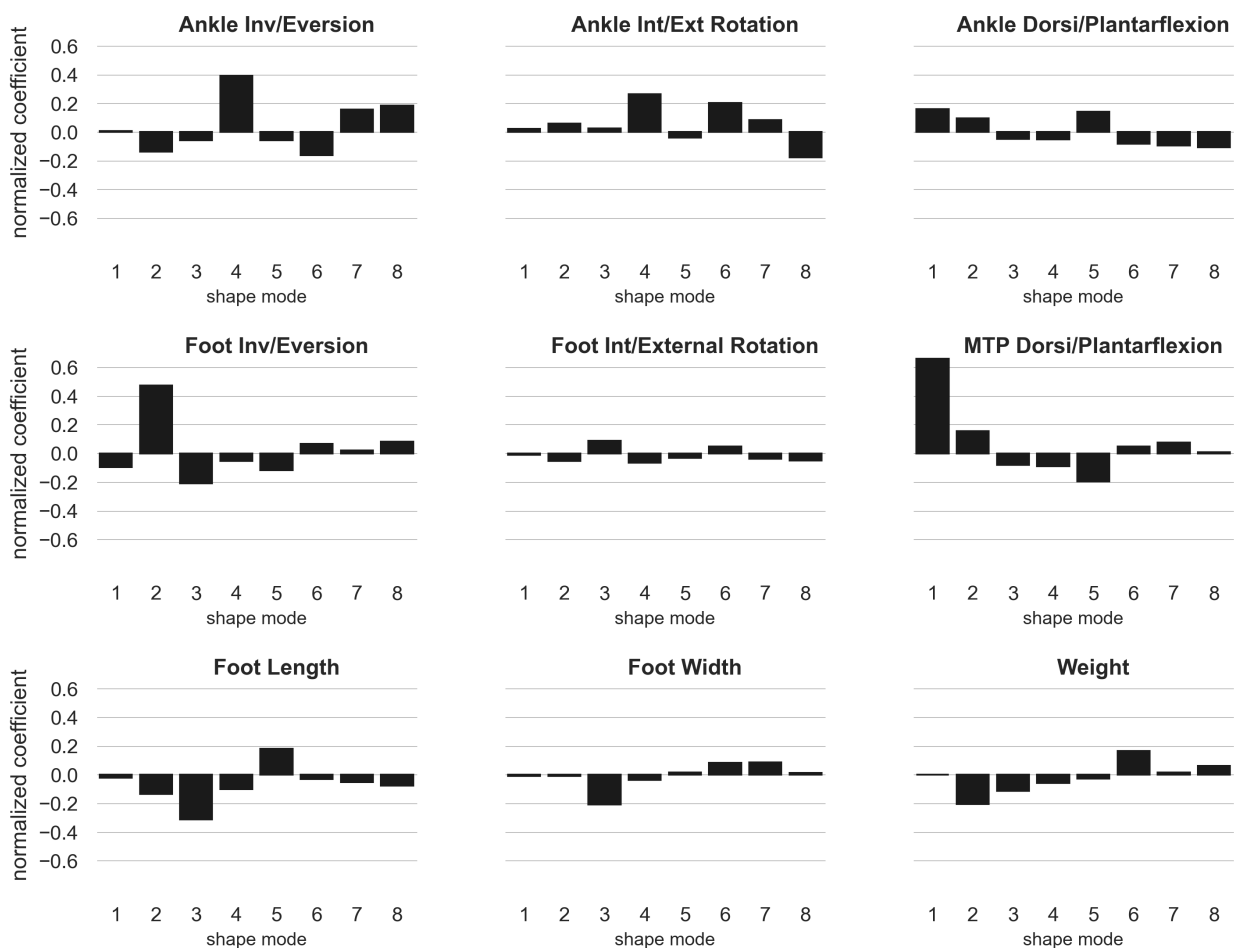
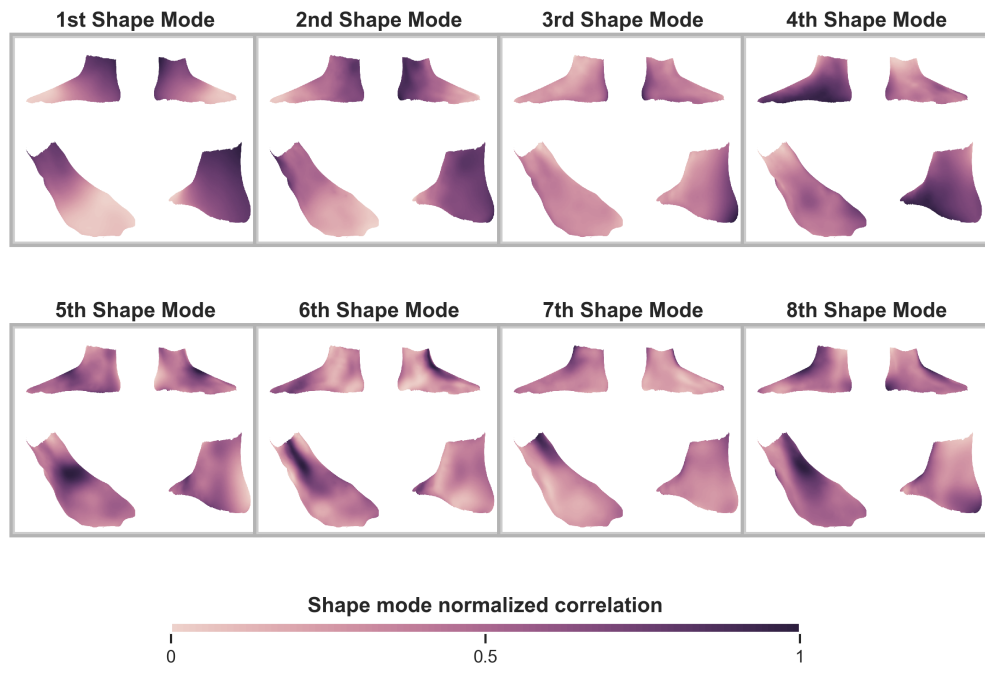


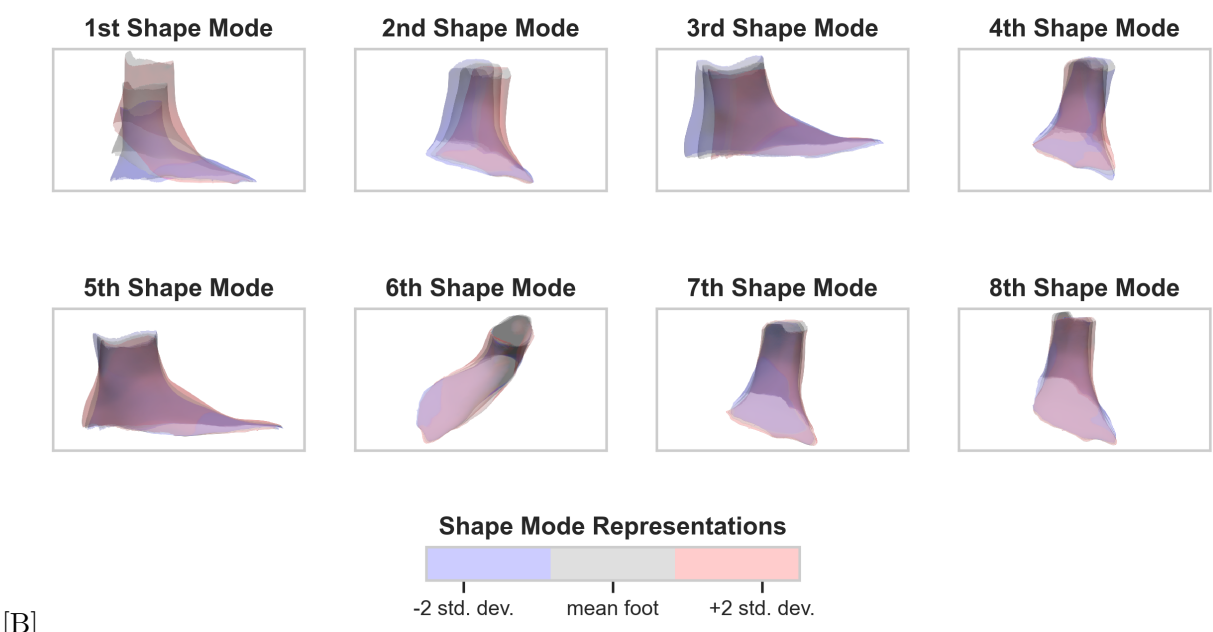
Figure 5.6: Each graph represents the predictor's effects on the shape mode by visualizing the model's normalized coefficients. Larger absolute values indicate a larger effect from the predictor on the shape mode.

Figures 5.3.2 shows each shape mode's axis represented on the mean foot, highlighting which areas of the foot are affected by deformations in each shape mode, and the ± 2 standard deviations of deformation along each shape mode overlaid on the mean foot.

Areas of foot affected by each shape mode



Deformations along each shape mode's axis



[[A] Each shape mode's principal axis represented as a heatmap overlaid on the mean foot and shown from 4 different point-of-views. The darker regions represent vertices which are most

 correlated with the shape mode's principal axis, and therefore see deformations in the shape mode.

[B] Foot shape deformation at +2 and -2 standard deviations along each shape mode's principal axis, overlaid on the mean foot. The point-of-view is set to highlight the major variance along each shape mode's axis.]

[A] Each shape mode's principal axis represented as a heatmap overlaid on the mean foot and shown from 4 different point-of-views. The darker regions represent vertices which are most correlated with the shape mode's principal axis, and therefore see deformations in the shape mode. [B] Foot shape deformation at +2 and -2 standard deviations along each shape mode's principal axis, overlaid on the mean foot. The point-of-view is set to highlight the major variance along each shape mode's axis.

5.3.3 Foot Shape Changes

This study was designed to construct and evaluate a parametric SSM in explaining and predicting dynamic foot morphology changes across the subject population. The model was able to predict dynamic foot shape across the subject population with an average RMSE of 5.2 ± 2.0 mm ~~and mean Hausdorff distance of 21.4 ± 7.4 mm. The disparity between RMSE and Hausdorff distance is due to scan edges, which have inherently high noise from depth camera capture.~~ For context, if all possible RMSE prediction error was accumulated to only affect length and width, it would be higher than the half-size step of the American shoe sizing system [88], but less than inter-brand variability of shoe length and shoe width [148]. Further, this error is lower than the RMSEs of other parametric SSMs that predicted static standing child body shape (mean=10.4mm) [109], dynamic shoulder deformation (mean=11.98mm) [78] and child torso shape (mean=9.5mm) [110]. Note though, that the presented model may have lower prediction errors due to the foot being a relatively smaller section of the body to model. Grant et al.'s model reconstructed internal foot bones with much lower RMSEs ~~and Hausdorff distances~~ from sparse anatomical landmarks (RMSE: 1.21-1.66 mm~~for various foot segments~~, ~~mean Hausdorff: 3.21-7.19 mm~~) [59] but was

trained with higher resolution MRI images. Other efforts to create statistical foot shape models did not incorporate parametric prediction of foot shape [35, 133].

~~The first, second, and fourth shape modes, accounting for a total of 86.7% of total variance, capture gross foot motion.~~ Foot motion during stance is dominated by MTP and ankle dorsi/plantarflexion [85], ~~which is~~ captured in the first shape mode (fig. 5.3.2). ~~The second and fourth shape modes capture gross changes in foot rotation from 5.3.2).~~ Shape changes in frontal and transverse plane movements at the MTP and ankle joints ~~planes~~ are captured in the second and fourth shape modes, respectively (fig. 5.3.2). ~~The second shape mode is most affected by foot inversion/eversion around the MTP joint.~~ The second shape mode also captures girth scaling at the ankle joint, as seen in (fig. 5.3.2) by how the ankle girth decreases along the axis, and is affected by weight (fig. 5.6). The fourth shape mode is affected by ankle inversion/eversion and internal/external rotation. Foot inversion/eversion, ankle inversion/eversion, and ankle internal/external rotation are expected to vary across the stance phase ([85]), which leads to the observed changes in gross movement. However, the 5.3.2). Movements captured in these shape modes are well correlated to the expected movement of foot during stance phase [85]. The second and fourth shape modes are slightly affected by foot length, which may suggest inter-individual effects in foot inversion/eversion, ankle inversion/eversion, and internal/external rotation during gait. There is a slight correlation between these angles and foot length (see supplementary figures), which may be due to differences in cadence when walking at the treadmill's set speed. Individuals were given time to acclimate to the treadmill's set speed, but the speed may not have been their preferred walking speed.

~~The Foot length scaling is captured in the third shape mode captures foot shape scaling at the rearfoot, as highlighted in (fig. 5.3.25.3.2).~~ Foot length shrinks when moving positively along the third shape mode (fig. 5.3.25.3.2), and thus has a negative effect from foot length. ~~There are also negative Negative effects from foot width and weight, which may be due to their correlation to foot length (see supplementary figures).~~ Rearfoot morphology along this shape mode has a more rounded shape in the negative direction, and a sharper shape in the positive direction (fig. 5.3.2). There is also a negative effect from foot inversion/eversion (fig. 5.6), indicating that with foot eversion, a

sharper rearfoot shape is expected. This may be due to foot eversion at heel-off [85], where the foot unloads from a rounder weight-bearing rearfoot to a sharper non-weight bearing rearfoot shape.

Midfoot girth increases and the rearfoot is rounder Longitudinal arch height is a significant factor in static [133, 35] and dynamic foot shape [129]. Due to limitations in the field-of-view of the cameras around the treadmill, arch height was not able to be directly measured. However, the instep area was found to rise along the fifth shape mode's axis (fig. 5.3.2). The fifth shape mode is 5.3.2), which is representative of the longitudinal arch apex. This was positively affected by foot length and negatively by MTP dorsi/plantarflexion (fig. 5.6). This suggests that static midfoot girth, suggesting that the instep height increases with foot length, and decreases through heel-off as the MTP dorsiflexes. Rearfoot morphology is rounder for longer foot lengths but gets sharper through heel-off with MTP dorsiflexion, much like in the third shape mode. Midfoot Jurca et al. found a similar relationship between static instep height and foot length, although there is still a wide variety of instep height in the population [73]. The drop in instep height is most likely related to the decrease in medial-longitudinal arch (MLA) angle, attributed to the windlass mechanism and measured through radiographs and optical motion capture [66, 25, 136]. Similarly, midfoot girth was previously found to decrease during stance phase compared to statically standing [60], most likely due to intrinsic and extrinsic foot muscle contraction [130, 54]. However, it was not noted where during stance phase midfoot girth decreases, but it can now be assumed it occurs during when taking this measurement over dynamic foot scans [60]. The presented model provides volumetric insight into where the drop in instep height occurs by identifying it in a shape mode, as well as allowing for its predictability from foot length and MTP dorsiflexion.

The heel was found to vary in the third and fifth shape mode's axis, varying from a rounded to a sharper shape along both axes. As the heel lifts off the ground at heel-off, the soft-tissue unloaded during gait and changes morphology [52]. At heel-off, there is foot eversion and MTP dorsiflexion [85], explaining the negative effects on the third and fifth shape modes, respectively (fig. 5.6).

The sixth shape mode captures girth Girth changes at the ankle, midfoot, and the medial MTP joint region medial MTP joints are captured in the second and sixth shape modes (fig. 5.3.2),

~~with girth increasing along the axis. There are positive effects from ankle internal / external rotation and weight, while there is a negative effect from ankle inversion/eversion (fig:SA2-coefs). Static MTP, midfoot, and ankle girth may therefore increase with 5.3.2).~~ Girths increase just prior toe-off with ankle internal rotation in the sixth shape mode, and eversion in the second and sixth shape modes (fig. 5.6). Girths are also increased with increased subject weight. Dynamic girth changes in these regions may occur as the ankle everts and internally rotates just prior to toe-off, where muscle activation is needed to push the foot off the ground. The foot is stiffened through tension in the MTP joints in order to prepare for toe-off [66], and the MTP joints are known to move relatively within the foot during gait [155, 86] which may be resulting in the increased girth at the MTP joint. A similar mechanism may be occurring at the ankle joint during ankle inversion and internal rotation, where tension from muscle activation prior to toe-off may cause increased girth.

The seventh and eight shape modes, accounting for 1.3% of total variance, capture girth increases near the medial malleolus along their axes (fig. 5.3.2). They are both positively affected by ankle inversion/eversion (fig. 5.6), and the eighth shape mode is further negatively affected by ankle internal/external rotation. This may suggest that the girth around the medial malleolus decreases prior to push-off, as the ankle everts and internally rotates. ~~model can inform last and footwear design recommendations for increased fit and comfort. Lasts are typically designed to shape the shoe for both fit and fashion, and are derived from static foot dimensions for a given size [88]. Previous work has proposed the use of 3D foot scans to inform last design [124], and even generate predicted individual shoe lasts [6]. The 3D meshes predicted by the model can generate lasts in various size grades and representative of shape changes during stance phase. For example, lasts can be constructed with a deformable or removable instep area, matched to the model's predicted reduction in arch height for a given foot length. Lasts could also feature a swappable heel element to ensure that rearfoot morphology is accommodated as the heel is off-loaded. Digital footwear design tools could also directly import the predicted meshes generated from this model for virtual fit tests: interaction models between the footwear design and the dynamic foot shape could ensure fit is consistent through motion. Shape changes identified from this model can also inform~~

footwear design. For example, the instep height drop may be accommodated with tensioned lacing, ensuring the foot is captured and cannot shift upward inside the shoe during heel-off. In addition, a heel counter can secure the changing morphology of the heel during heel-off, preventing heel rise within the shoe. While such elements are already found in many commercially available shoes, the presented model validates their importance and provides a framework for iterating on their design.

5.3.4 Study Limitations

A number of limitations in this study should be noted. The elastic-net method is able to retain cross-correlated predictors, but still requires some bias in the dataset to predict scenarios where cross-correlated predictors are independent [162]. Therefore, the presented model may not be valid for predicting changes in morphology ~~due to from~~ independent changes in joint angles outside of stance phase, or ~~for from~~ variance in foot width or weight compared to foot length not captured in the subject population.

The model did not capture ~~differences between male and female feet. Studies found that~~ sex differences in foot shape; ~~studies found that these differences~~ after scaling for foot length were not significant [81, 15, 35], or were small in magnitude [156, 83]. No ~~subject demographic~~ data was collected to ~~account for differences in foot shape~~ ~~analyzed foot shape differences~~ due to ethnicity [73]. ~~No data was captured on the foot's plantar surface due to limitations with the scanning system; therefore foot arch changes were not captured. Data captured around the toes had high noise, which necessitated smoothing the toes in the template to ease fitting~~
~~Data at the toes was noisy, necessitating smoothing the template's toes to ease fitting.~~ Plantar foot shape was not captured, which is also known to vary with foot shape and loading [95]. Future advances in 4D scanning may alleviate some of these concerns, and also allow for expansion of this model to higher frequency foot motions, such as running
~~scanning technology may improve data quality and allow for capture of arch shape and plantar shape for further analysis.~~

5.3.5 Study Conclusions

The observed girth changes at the ankle joint, medial malleolus, midfoot, and MTP joint can be directly mapped to spacesuit footwear design recommendations to reduce instances of heel-lift. During heel-lift, the heel rises inside the boot, resulting in the midfoot rotating upward around the MTP-joint much like after the heel-off phase in gait. This can only occur if there is empty space above the midfoot; if the boot's internal shape were perfectly fit to the foot's shape, the foot would not be allowed to move inside the boot. Unlike some terrestrial footwear which can rely on the elasticity of uppers to continuously capture the foot, the stiff nature of a pressurized spacesuit boots does not allow for its upper to continuously conform to the foot if the foot changes shape. The study showed that midfoot girth decreased as the MTP joint is dorsiflexing after heel-off in the fifth shape mode. Therefore, a spacesuit boot should have a mechanism to conform to this volume change to reduce empty space above the midfoot and therefore reduce instances of heel-lift. Heel counters are also designed into many terrestrial boots to ensure the heel stays index through motion; a well-designed heel-counter could also help reduce heel-lift. Rearfoot morphology changed from a rounded shape to a sharper shape with MTP joint dorsiflexion in the fifth shape mode, suggesting that a heel-counter may need to account for this shape change to properly capture the heel. A combination of midfoot capture and an improved heel-counter that account for these morphological changes can work together to reduce instances of heel-lift in the spacesuit boot.

5.4 Analysis of Dynamic Instep and Arch Height Changes



~~While the~~ The dynamic foot shape model provides insight into how regions of the foot change shape due to motion or anthropometry, ~~it only outputs foot shapes and not linear or circumferential foot measurements~~. One of the primary findings in this study from the model was the decrease in midfoot girth arch height during stance phase, following by an increase through heel-off; ~~this region is represented by the linear foot measurements of instep height and instep girth. Translating the foot-shape changes in the midfoot to linear measurements will provide a basis for footwear designers~~

~~to ensure their uppers have the range to conform to the midfoot throughout gait. Specifically for this thesis, this linear.~~ However, the nature of a SSM is that it only outputs foot shapes and not linear or circumferential foot measurements. Therefore, the magnitude of arch height change was not characterized in this model. Characterizing arch height changes will assist in the spacesuit boot design, as this measurement will provide a baseline for engineering a conformable upper into a spacesuit boot to reduce which reduces empty space above the midfoot and thereby may reduce heel-lift. In addition, comparing

Arch height, however, is not a primary measurement in terrestrial footwear fit.

Lasts are traditionally made in a single reference size, and then either geometrically, arithmetically, or proportionally scaled larger and smaller to match other user sizes based on foot length [88]. This process results in other foot dimensions being scaled with the same proportion as foot length. However, arch height has little correlation with foot length [67]. Arch height is not a measurement used in the grading of shoe sizes, as such customers are not able to select shoes which fit their arch with quantitative fit metrics. Instep height, which is taken near the foot's arch, may be targeted in last design, but is also not used in grading. Furthermore, foot measurements defining shoe sizes are taken statically, and do not account for the dynamic changes in ~~these measures to their static population range will allow for future sizing analyses to include how much instep height conformal range is needed for each shoe size.~~ foot shape due to the foot's loading during gait.

~~Volumental AB, a footwear research company, has developed a database of 1.2 million footwear consumer static foot scans around the world [73]. Analysis of this database showed that The arch changes shape dynamically during gait, thus exacerbating difficulty in accommodating its shape during movement. Medial longitudinal arch (MLA) shape changes are thought to be caused by several mechanisms.~~

~~Hicks used radiographs to show that the foot's arch drops and decreases in angle while it is loaded during early and mid-stance, and rises and increases in angle during late stance [66]. They hypothesized that a stiff plantar fascia results in a windlass mechanism, where the plantar fascia is pulled towards the toes as the toes dorsiflex during late stance phase. This shortens the arch~~

and raises its height. Additionally, Ker et. al hypothesizes that the arch behaves like a spring, where it is compliant and stiff during early and mid-stance, and then recoils in late stance to increase in height and assist in propulsion [75]. They also observed this arch height drop during early and mid-stance. Similarly, optical motion capture techniques have shown that the MLA angle increases and arch height drops in during early and mid-stance, followed by the MLA angle decreasing and arch height rising in late-stance [25, 28, 85, 136]. The arch's dynamic motion can be attributed to a combination of the windlass and arch-spring mechanisms, providing a physical explanation to the arch's dynamic motion [150, 151]. The rise and fall of the arch are reflected as shape changes in the foot's instep area; this was found to be the largest variation in foot shape between loaded and unloaded feet [129].

Customers aiming to find footwear that fits their foot shape may face difficulties due to the lack of arch or instep height as a fit metric and the dynamic nature of the arch itself. Arch and instep height variation can be accommodated for in footwear through lacing and upper design. Customers therefore may need to try on various shoes while searching for an upper design that matches their arch and instep height. Customers may also adjust the fit of the arch and instep in each shoe they try on with lacing until they are satisfied with their fit. Lacing modifies how the shoe's upper sits on the wearer's foot, frequently implemented above the wearer's arch and instep. Lacing can provide a level of customization to arch and instep fit, especially when compared to an elastic shoe upper [69]. Proper lacing  can also ensure comfort and performance during activities [63, 64, 116]. Furthermore, tensioned lacing could be used to ensure that dynamic fit is maintained as the arch moves through gait [116]. Investigating how both static and dynamic arch height may relate to other foot measurements could improve footwear design, such as by scaling lasts more accurately to accommodate arch height and provide customers with a guide in selecting shoes that fit all aspects of their foot shape.

To address this gap in footwear design, understanding the magnitude of foot shape changes at the arch may be used. The arch sits at the middle of the foot, just under the instep region. Therefore, it is expected that any change in arch height and MLA angle would affect instep height.

There is also opportunity to investigate if dynamic arch height changes are affected by the subject's static foot measurements, and if the instep height measurement is analogous dynamically to the arch height measurement. The objective of this research is to evaluate whether dynamic instep height changes can be correlated to static foot measurements. This research hypothesizes that 4D scanning can be used to quantify instep height changes, and that dynamic instep height change is correlated to static instep height, foot length, and foot width.

5.4.1 Methods

Instep height measurement was evaluated as an appropriate measure to assess static and dynamic arch height in static scans. A strong correlation between these measurements allows for comparison to arch height measures since instep height is measured near the location of the MLA. Instep height measurements were first correlated to arch height measurements using a subset of the median 90% of the population had a range of 16.2 mm [73]. In collaboration with Volumental AB, The 3D static foot scan measurement dataset from [73] (Swedish Ethics Review Authority reference No. 2019-03243). The dataset was down-sampled to only include length classes in the 4D scan dataset used for the aforementioned dynamic foot shape model will be expanded to output instep height measurements, with the method outlined in Jurea et al. [73], across the kinematic variables, foot length. Instep height measurements were taken for each foot scan by taking the height of the frontal cross-section at 55% of foot length from the heel [73]. Arch height measurements were taken at the frontal cross-section at 45% of foot length from the heel [73]. From this cross-section, the height from the ground to the foot is taken at 25% of the foot's width at this cross-section from the lateral side. Pearson correlation coefficients were computed between the instep height and arch height within this dataset.

As the 4D foot scans did not include the foot's plantar surface, a new method for measuring instep height was defined, summarized in fig. 5.7. A virtual landmark, labeled as the middle metatarsal head, was defined as halfway between the medial and lateral metatarsal heads. Then, a triangle was defined on the scan's sagittal plane, with its base defined as the vector from the pterion

to the middle metatarsal head. The triangle's height was defined as the orthogonal distance from this vector to the instep landmark; this height was recorded as the scan's instep height. While the instep height landmark may not be perfectly aligned with the pterion-middle metatarsal head vector, this method ensures that the instep height measurement is always taken perpendicular to the base of the defined triangle in the foot's sagittal plane. Despite the data set limiting the measurement technique from following the traditional methods of measuring instep height from the literature [73], this method does represent the height of the foot at the instep area when the plantar surface of the foot is not available as a reference.

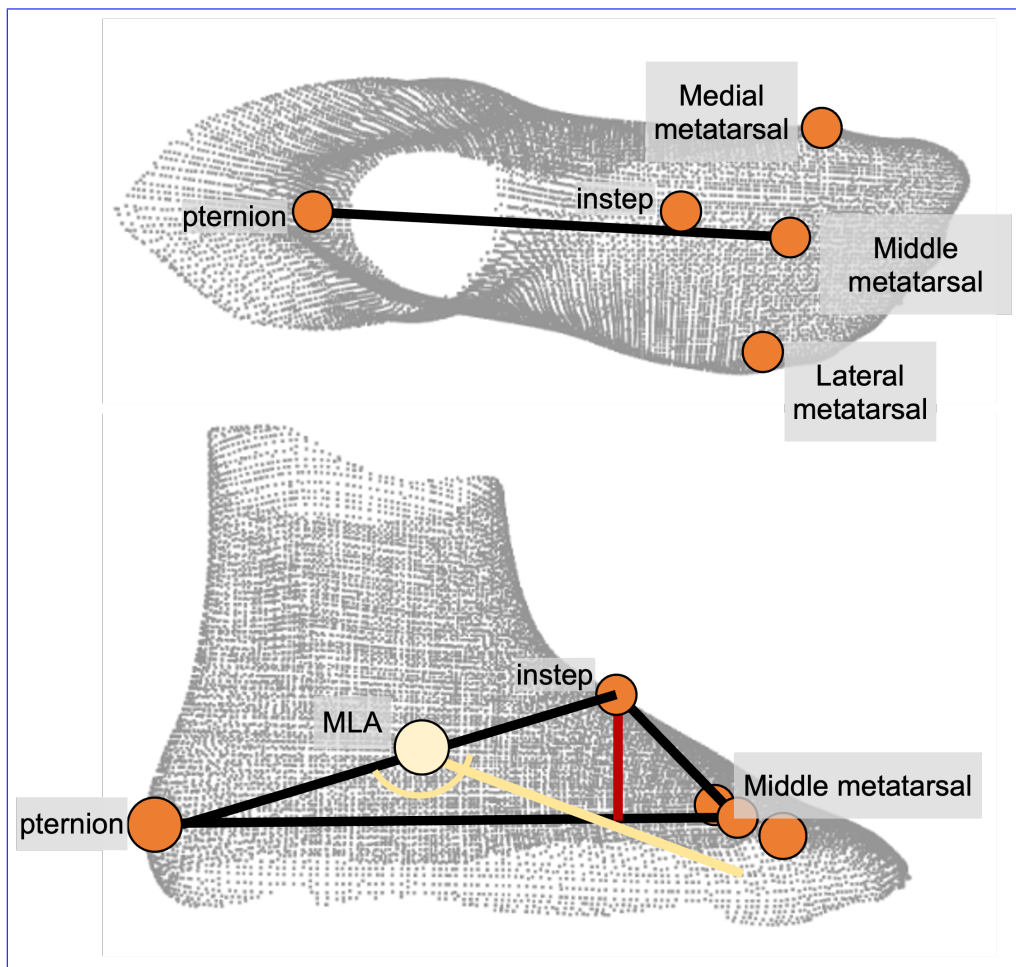


Figure 5.7: Landmarks and vectors used for instep height measurement, shown in top and side views. The principal foot axis is defined from the pterion to the middle metatarsal head landmark (top). A triangle is defined with a base between the middle metatarsal head and the pterion, and an upper vertex at the instep landmark (bottom). The height of this triangle (red) is taken as the instep height. The MLA location is also shown for comparison.

For each subject, the instep height measurement over stance phase was filtered with a 2nd order Butterworth low-pass filter, with a cutoff of 15 Hz, to reduce measurement noise. Mid-stance instep height was defined as the instep height taken halfway between heel-strike and ~~foot width of the dynamic model's subject population. When compared to toe-off for all subjects, representative of the static instep height. The late-stance instep height measurement was noted as the highest instep height measurement between mid-stance and toe-off. The difference between these two instep height measurements was calculated for each subject as the dynamic instep height change.~~ The correlation coefficient was computed for each scan within each subject between instep height and MTP joint angle. The MTP joint angle was chosen for correlation analysis as the hypothesized windlass mechanism for arch height rise is dependent on the MTP joint angle [66]. Correlation coefficients were also computed between all subjects' dynamic instep height change and their foot lengths, foot widths, and static instep heights. Subjects' maximum instep height changes were compared to subjects' foot lengths, foot widths, and static instep heights to identify if there are any trends which predict the maximum instep height change.

5.4.2 Results

Analyzing Volumental's static scans found a correlation coefficient of 0.70 and 0.71 was found between instep height and arch height for females and males, respectively. Instep height was calculated for subjects with dynamic scans and compared to their MTP joint angles. The relationship between selected subject's MTP joint angle throughout stance phase, and their measured instep height, is shown in fig. 5.8. For most subjects, the instep height drops from early to mid-stance, and then rise in late stance with the MTP joint angle. Correlation coefficients between the calculated instep height and MTP joint angle from dynamic scans for each subject are also noted in fig. 5.8. Twenty-five of the thirty subjects had high correlations ($r^2=0.73\pm0.10$) between their instep height and the MTP joint angle. These subjects had a mean instep height difference of $15mm\pm4mm$. The remaining five subjects (Subjects 2, 16, 21, 22, and 29) had low to no correlation

$(r^2=0.11\pm0.36)$ between their instep height and the MTP joint angle across the gait cycle. These subjects' data was manually examined for anomalies, but none were found.

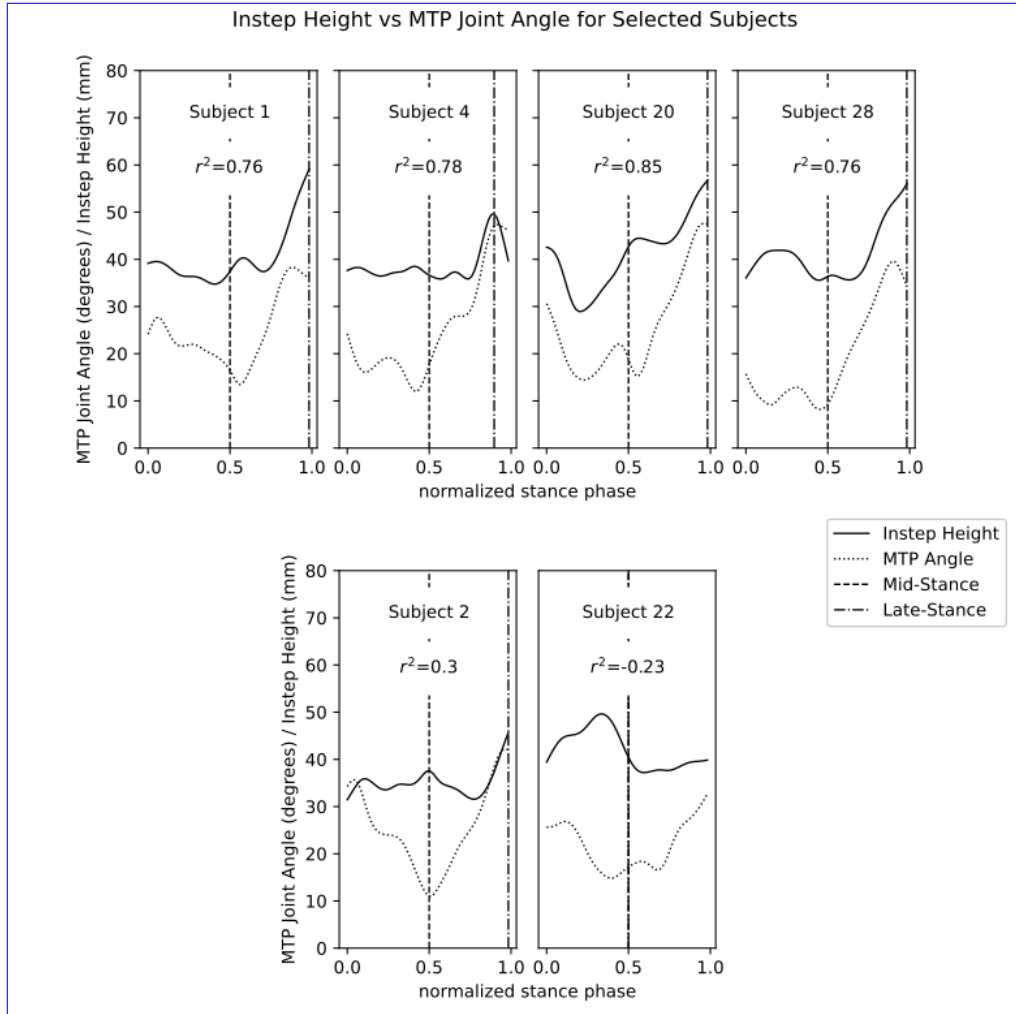


Figure 5.8: Correlation between selected subjects instep height and MTP joint angle over stance phase. Subjects with high correlation between their MTP joint angle and instep height are shown on the top row. Subjects with lower correlations between their MTP joint angle and instep height are shown on the bottom row. Locations of where mid-stance and late-stance instep height values are taken for each subject are highlighted as vertical lines. The Pearson correlation coefficient for each subject is shown on their graph.

Maximum instep height change was found to be 53.7 ± 4.44 mm for the static measurements done by Jurea et al. [73], tolerances for instep height can be defined across the population; specifically, the range needed to capture the median 90% population for each foot length class. In this thesis, and in collaboration with Volumental AB, these results will be extended to instep

~~girth. Findings from this study will be related to spacesuit design variables.~~ 25 subjects with high correlations between instep height change and MTP joint angle. ~~tbl. 5.2 shows the correlation coefficients between the maximum instep height changes and foot length, foot width, and static instep height for these subjects.~~

~~As a stretch goal, this analysis can be repeated for the measures of foot length.~~

Table 5.2: Pearson correlation coefficients between maximum instep height change and subjects' anthropometric measurements

Anthropometric measurement	Correlation to maximum instep height change
Foot Length	0.18
Foot Width	0.18
Static Instep Height	-0.16

5.4.3 Translating Instep and Arch Height to Footwear Design

~~A new measurement technique was proposed to analyze 4D foot scans for changes in instep height due to the dynamic nature of the MLA during gait. This technique provides a normalized way to~~ This method does not require the foot's plantar surface to be captured, enabling collection of scans on a treadmill or across a walkway. The medial longitudinal arch is expected to drop in height during early to mid-stance, and then rise during late stance [66, 75, 25, 28, 85, 136, 151, 150]. A similar pattern was seen in the instep height measurement. Across most subjects, the instep height measurement drops during early and mid-stance, and then rises during late-stance. Therefore, it can be hypothesized that the rise and fall of the MLA changes the instep height of the foot.

~~Since the collected 4D scans do not include the plantar surface, the method used to measure instep height is slightly different than traditional methods.~~ The traditional method of measuring instep height is taken with respect to the ground when the foot is flat, which cannot be done with dynamic 4D scans captured on a non-transparent surface. This is due to the foot lifting off the ground after heel-off and therefore not having a reference for the measurement. The proposed

method provides the instep height with respect to a virtual vector drawn from the middle of the metatarsal heads to the pterion. This measurement technique is still valid for quantifying instep height changes as the arch is located above this virtual vector, and provides a standardized measurement across all subjects' dynamic scans. Therefore, the reported changes in instep height may still be accurate even when the full instep height measurement is not taken.

Five of the thirty subjects did not have a strong correlation between their instep height and the MTP joint angle. No anomalies with the instep height measurement were identified after manually reviewing the subject's 4D scans. In addition, manually reviewing the subject's MTP and ankle joint kinematics also did not reveal any differences. These subjects' static instep heights were also similar to subjects whose instep height had a strong correlation to the MTP joint angle. Since instep height was found to be highly correlated to arch height, these subjects' arch height also cannot explain why they have low correlations to the MTP joint angle during stance phase. However, some of these subjects (Subjects 2, foot width, and heel width. While this goal is not a thesis contribution, this opens the door to understanding how much footwear needs to be conformal to the user's foot shape; identifying variables that will help prioritize footwear design measures²¹, and 29) still have a rise in instep height in late stance that is characteristic of the arch height rise due to the windlass and arch-spring mechanisms [66, 75]. The low correlation suggests that for these subjects, instep height changes may be occurring primarily due to the arch spring hypothesis rather than the windlass hypothesis [75]. On the other hand, subjects 16 and 22 had little to no change in instep height. The five subjects in the group without a strong correlation between instep height and MTP joint angle may have a foot structure that responds differently compared to the other subjects', or their arch may not be aligned with the location at which the instep height measurement was taken.

Static arch height has been previously shown to have low correlation to foot length [67]. In this study, no strong correlations were found between instep height changes and other foot anthropometric measurements, suggesting that the instep height change is another mode of variation in foot shape. In addition, there were some subjects in this study who did not have

a strong correlation between arch height and MTP joint angle. Both findings suggest that arch and instep height varies inter-individually.

This finding has many implications for footwear design. Geometric, proportional, and arithmetic last grading techniques vary the dimensions of the master last by a percentage of the last, by fixed proportions in various dimensions, or by a fixed increment in various dimensions, respectively. However, these grading techniques cannot consider the variability of static arch height and dynamic instep height, as this variability seems to be different for everyone. Therefore, adjustable mechanisms at the instep area to personalize fit may be necessary to allow footwear to fit a large population properly. In addition, these mechanisms should be adaptable to the dynamic changes in instep height during gait. A fixed instep area might result in the foot lifting within the shoe, also known as heel-lift, just before heel-off when the instep height has dropped and there is empty space in the shoe.

The tongue and shoelaces can provide adjustment at the instep area independent of shoe size. Shoe lacing provides tension over the tongue of the shoe [63, 113], which ensures that the tongue stays snug on your instep area. Findings from this study show that the tongue should accommodate at least 20 mm of movement to fit most subject's instep height changes. Individuals can adjust the lacing to best accommodate their static instep height. Shoe lace tension can also be adjusted by varying the number of eyelets and lacing pattern used by the individual [63, 64]. Therefore, shoelace tension can be adjusted by an individual to match their dynamic instep height and arch function. An individual with large instep height changes during stance phase could have higher-tension lacing to ensure the tongue can rise in late stance and then collapse again during the following step's mid-stance phase. Alternatively, an individual with low instep height changes may not need to tension their shoelaces as high. Therefore, shoelaces can allow individuals from this study with high correlation between their instep height and MTP joint angle, and those with low correlation between their instep height and MTP joint angle, to adjust shoe fit to their foot shape and dynamic nature. Advanced shoe lacing concepts have also been shown to reduce in-shoe motion, which could be due to their superior tension provided by these concepts [116, 98].

These concepts could also be providing an easier mechanism for the wearer to adjust the tension appropriately; these wearers could adjust the tension to their liking in an easier fashion to ensure that they are minimizing in-shoe motion while still maintaining comfort.

It should also be noted that the dynamic instep height measurement may not be only due to the MLA. It has been suggested that the foot's transverse arch can also change in curvature due to load, and also affect the foot's stiffness [144]. As the transverse arch is also located close to the region of the foot where the instep height is measured, it may also have a dynamic component that is contributing to the rise of the instep during gait. Further studies of the transverse arch mechanics may be needed to confirm this.

5.5 Summary

A 4D scanning system was developed to capture dynamic foot shape changes, and was used to collect data for development of the model. To the authors' knowledge, this is the first parametric foot SSM that captures and reconstructs dynamic motion. The model was able to identify specific changes in foot morphology as they related to subject and kinematic parameters, and suggest spacesuit boot design techniques to reduce instances of heel-lift. ~~Along with these techniques, the model is able to reconstruct a full 3D model when parameter values are provided, which offers a design starting point for constructing a planetary spacesuit boot prototype in Specific Aim 3.~~

~~To date, all data collection for Specific Aim 2 has been completed. A journal paper detailing the development of the 4D scanning system was published in the Journal of Open Source Software [20]. A journal paper detailing the development of the model is currently under review, and has been released as a preprint [21]. The instep height and instep girth analysis is just starting and will be presented in a future journal paper. The dynamic shape changes around the arch were further studied, as the arch is a challenge to fit properly. The instep height measurement was found to closely correlate to the arch height measurement. A new method of measuring instep height on dynamic foot scans without a plantar surface was developed. Strong correlations were found between the MTP joint angle and the instep height, reinforcing the dynamic nature of the MLA~~

angle dynamics. However, correlations were low between instep height change and static foot measurements, highlighting the need for adjustable and potentially dynamic lacing integrated into the upper to maintain fit throughout the gait cycle.